NASA Technical Paper 1242

Simulation Study of the Oscillatory Longitudinal Motion of an Airplane at the Stall

William H. Phillips

AUGUST 1978

NASA

NASA Technical Paper 1242

Simulation Study of the Oscillatory Longitudinal Motion of an Airplane at the Stall

William H. Phillips
Langley Research Center
Hampton, Virginia

National Aeronautics
and Space Administration

Scientific and Technical Information Office

1978

SUMMARY

Hybrid simulation studies of the longitudinal motion of a straight-wing airplane at the stall have been made to investigate the effect of hysteresis in the development of lift and pitching moments on the wing as a function of angle of attack on the occurrence of longitudinal oscillations at the stall. Flight data for the simulated airplane and for various other airplanes are shown for comparison. The results show that oscillations similar to those measured in flight may be obtained by incorporating hysteresis in the lift and pitching-moment curves. More complete wind-tunnel data on the dynamic stall characteristics of an airplane would be required to predict these longitudinal oscillations more accurately.

INTRODUCTION

A typical motion of an airplane as it gradually approaches the stalled condition consists of some random oscillations about all three axes followed by a rather abrupt roll. The rolling motion which occurs in most of the airplane tests has been explained on the basis of the static lift curve. That is, if the angle of attack increases into a region where the lift-curve slope is negative, any downward movement of a wing tip results in loss of lift from that wing tip and produces a divergent rolling motion. More complex effects, such as nonlinear roll damping, loss of directional stability, and other aerodynamic characteristics, may, of course, be involved in providing a complete explanation of the lateral behavior at the stall. In some cases, however, particularly in power-off conditions, the rolling motion either does not occur or may be prevented or delayed by use of the rudder. In this case, the airplane often performs a divergent short-period pitching oscillation. In cases in which a divergent longitudinal oscillation occurs, the behavior cannot readily be explained on the basis of the static aerodynamic characteristics. Hysteresis in the lift and moment curves, which has frequently been observed to occur during dynamic motions in the range of angles of attack near the stall, is probably required to explain the pitching oscillation. Similar oscillatory motions under conditions of separated flow have been observed in other applications, such as torsional flutter of compressor blades and oscillations of buildings and towers.

Some examples of flight data records from stall tests in which the airplanes exhibited longitudinal pitching oscillations are given in figures 1 to 4. Pilots sometimes call these oscillations "bucking" or "porpoising." In all these cases, the oscillations

occurred in the power-off condition. With power on, the action of the slipstream prevented stalling at the root section of the wing and the airplanes generally exhibited lateral-directional divergence before any regular pitching oscillation was apparent.

In the stall shown in figure 1, made in the power-off, flap-up condition, the pilot gradually applied increased upward elevator deflection but made no effort to control the airplane laterally. A slowly divergent short-period longitudinal oscillation of about a 2-sec period developed during the stall. After about five cycles of oscillation, the airplane rolled off abruptly. These records are from previously unpublished data.

The records of figures 2(a) and 2(b), also from previously unpublished data, show stall behavior somewhat similar to that shown in figure 1, but on a high-wing rather than a low-wing light airplane. Figure 2(a) for the power-off, flap-up condition, shows an oscillation quite similar to that of figure 1. In the flap-down condition shown in figure 2(b), the oscillation has a larger amplitude and a longer period than that shown in figure 2(a).

The data of figures 3 and 4 show stall behavior involving short-period longitudinal oscillations, but on airplanes of different types. Records of the power-off stall of a light bomber airplane from reference 1 are shown in figure 3. The oscillation appears to be similar to that of the general-aviation airplane of figure 3, although it has a somewhat longer period probably because of increased inertia in pitch. The light bomber airplane had air inlets for the radiators in the wing leading edge between the fuselage and nacelles. This feature probably contributed to an early stall of the inboard sections in the power-off condition, which resulted in a stall involving primarily longitudinal motion.

Records of the power-off stall of a modified light airplane from reference 2 are shown in figure 4. The modifications to the airplane were intended to prevent the attainment of a complete stall. In this case, a longitudinal oscillation of much longer period develops, which appears to be a divergent phugoid motion rather than a short-period oscillation.

In all the cases shown, the type of stall involving primarily longitudinal motion was considered desirable, inasmuch as the oscillation provides warning of the stall and can be readily stopped by the application of downward elevator deflection. Buffeting also provides a desirable type of stall warning, and usually accompanies the longitudinal motion because of the flow separation at the center portion of the wing.

Although many wind-tunnel investigations of wings have been made to determine dynamic stalling characteristics of airfoils, no known attempts have been made to use these data in predicting the dynamic longitudinal motion of an airplane at the stall. Also, it appears that no tests are available that determine dynamic characteristics in pitch of complete airplane configurations. The present investigation is an exploratory study using a hybrid computer to determine how well the longitudinal motion at the stall can be simu-

lated. Various assumptions were made regarding the dynamic stall behavior of the wing. The airplane chosen for the simulation is the single-engine general-aviation airplane for which flight data are given in figure 1. The occurrence of longitudinal oscillations at the stall is believed to depend primarily on the assumptions made regarding aerodynamic hysteresis rather than on the choice of inertia and aerodynamic characteristics of the airplane. The particular choice of the airplane for the study is not, therefore, considered to be of very great importance.

Because of lack of detailed knowledge of the dynamic stall process, the results are not expected to duplicate precisely the motion of a complete airplane. Stalling characteristics are strongly affected by the details of a particular configuration. Specifically, for cases in which a longitudinal oscillation develops at the stall, the wing is usually stalled only at the root. Lateral stability is retained because the tips remain unstalled. Important effects on the downwash at the tail would also be expected under these conditions. Wind-tunnel data are not available, however, to predict the details of the forces, moments, and downwash on an airplane during dynamic stall when only the root sections reach the stalled condition. Furthermore, stalling is known to be characterized by the occurrence of randomly varying forces and moments superimposed on an underlying stall behavior (ref. 3). These randomly varying forces and moments are not well understood and are not included in the present simulation.

SYMBOLS

C_D drag coefficient, $\dfrac{D}{\frac{\rho}{2} V^2 S}$

$C_{D,o}$ profile drag coefficient

C_L lift coefficient, $\dfrac{L}{\frac{\rho}{2} V^2 S}$

$C_{L,max}$ maximum lift coefficient

C_N normal-force coefficient, $\dfrac{F_N}{\frac{\rho}{2} V^2 S}$

C_m pitching-moment coefficient, $\dfrac{M_Y}{\frac{\rho}{2} V^2 S c}$

c	wing chord, m
D	drag, N
F_N	normal force, N
g	acceleration of gravity, m/sec^2
I_Y	moment of inertia in pitch, $kg\text{-}m^2$
k	reduced frequency, $\frac{\omega c}{2V}$, rad
L	lift, N
l_t	tail length, m
M	Mach number
M_Y	pitching moment, N-m
m	mass, kg
n	normal acceleration, g units
P	engine power, kW
P_m	maximum engine power, kW
p	rolling velocity, rad/sec
q	pitching velocity, rad/sec
R	Reynolds number
r	yawing velocity, rad/sec
S	wing area, m^2

S_t	tail area, m^2
T	thrust, N
t	time, sec
V	airspeed, m/sec
W	weight, N
x	center-of-gravity location, m
x_o	location of aerodynamic center of wing-fuselage combination, m
α	angle of attack, rad or deg
β	angle of sideslip, deg
γ	flight-path angle, deg
δ_a	aileron angle, deg
δ_e	elevator angle, deg
δ_r	rudder angle, deg
δ_t	throttle position, fraction of full throttle
ϵ	downwash angle, deg
η	propeller efficiency
ρ	air density, kg/m^3
τ	elevator effectiveness factor, $\frac{\partial \alpha}{\partial \delta_e}$ with $C_{L,t}$ held constant
ω	circular frequency, rad/sec

Subscripts:

t	tail
w	wing

Derivatives indicated by subscript notation:

$$C_{L_\alpha} = \frac{\partial C_L}{\partial \alpha}, \quad C_{m_\alpha} = \frac{\partial C_m}{\partial \alpha}, \text{ etc.}$$

Dot over a quantity indicates derivative with respect to time.

EQUATIONS USED IN SIMULATION

The equations of motion used in the simulation of longitudinal motion are programed in the analog portion of a hybrid computer. The equations are set up in a wind axis system shown in figure 5. Thrust is considered to be the component of propulsive force aligned with the velocity vector. The equations are as follows:

$$\dot{V} = \frac{T - D}{m} - g \sin \gamma$$

$$\dot{\gamma} = \frac{L}{mV} - \frac{g \cos \gamma}{V}$$

$$\dot{q} = \frac{M}{I_Y}$$

$$\dot{\alpha} = q - \dot{\gamma}$$

The aerodynamic forces and moments for unstalled flight are given by the following equations:

$$L = C_L \frac{\rho}{2} V^2 S$$

$$D = C_D \frac{\rho}{2} V^2 S$$

$$T = \frac{P\eta}{V}$$

$$M_Y = C_m \frac{\rho}{2} V^2 Sc$$

where

$$C_L = C_{L,w} + C_{L,t}$$

and

$$C_{L,w} = \alpha C_{L_{\alpha,w}}$$

$$C_{L,t} = C_{L_{\alpha,t}} \frac{S_t}{S}\left[\alpha\left(1 - \frac{\partial\epsilon}{\partial\alpha}\right) + q\frac{l_t}{V} + \delta_e\tau\right]$$

$$C_D = C_{D,o} + \alpha^2 C_{D_{\alpha 2}}$$

$$P = \delta_t P_m$$

$$C_m = C_{m,w} + C_{m,t}$$

and

$$C_{m,w} = \alpha C_{L_{\alpha,w}}\left(\frac{x - x_o}{c}\right)$$

$$C_{m,t} = -C_{L_{\alpha,t}} \frac{S_t}{S}\frac{l_t}{c}\left[\alpha\left(1 - \frac{\partial\epsilon}{\partial\alpha}\right) + q\frac{l_t}{V} + \delta_e\tau\right]$$

The representation of hysteresis in the lift, drag, and pitching moment of the wing beyond the stall is accomplished by generating these quantities in the digital portion of the hybrid computer. When the lift coefficient is a nonlinear function of angle of attack, downwash is generated in proportion to lift coefficient rather than angle of attack, and the

constant of proportionality is chosen to give the same value of $\partial\epsilon/\partial\alpha$ below the stall as in the linear case. For the digital simulation, then

$$C_{L,t} = C_{L_{\alpha,t}} \frac{S_t}{S}\left(\alpha + q\frac{l_t}{V} + \delta_e\tau - C_{L,w}\frac{\partial\epsilon}{\partial C_L}\right)$$

where

$$\frac{\partial\epsilon}{\partial C_L} = \frac{\partial\epsilon/\partial\alpha}{C_{L_{\alpha,w}}}$$

$$C_{m,t} = -\frac{l_t}{c} C_{L,t}$$

In cases for which the digital computer is used to generate the force and pitching-moment coefficients, the downwash at the tail is delayed by the time for the flow to go from the wing to the tail. This delay is accomplished by storing the previous 50 values of lift coefficient at intervals of 0.01 sec and recalling the value at the appropriate delay interval l_t/V for calculating the downwash.

Numerical values of airplane characteristics used in determining the coefficients of the equations used in the simulation are given in table I. These values are representative of a single-engine, low-wing, general-aviation airplane.

PROCEDURE

Because the hybrid simulation represents the longitudinal motion of the subject airplane throughout its speed range and incorporates provisions for throttle and elevator inputs, the airplane could be "flown" manually through any desired longitudinal maneuvers. For obtaining consistent data, however, the inputs were put in by the computer as ramp motions of the elevator with varying rates. The throttle position was found to have little effect on the motion at the stall. The runs presented were, therefore, made with a throttle setting of zero. The data were recorded on a strip-chart recorder. Data are presented only for a ramp motion of the elevator of 0.016 rad/sec (0.917 deg/sec) starting from a trim condition slightly below the stall.

DATA ON DYNAMIC STALL CHARACTERISTICS OF WINGS

Although numerous studies have been made of the aerodynamic forces and moments on wings oscillating in the stalled flow region, the ability to model these characteristics on a particular wing performing arbitrary motions is quite limited. Surveys of the research on dynamic stall characteristics are given in references 4 and 5. Because of limitations of test equipment, most of the existing studies are confined to low values of Reynolds number and to two-dimensional, unflapped airfoils performing sinusoidal oscillations through specified ranges of angle of attack at a limited number of frequencies. Typical variations of normal-force coefficient and pitching-moment coefficient with angle of attack on two-dimensional airfoils during these oscillations are shown in figure 6. These data are taken from references 4 and 6. Attempts to model the flow phenomena involved in dynamic stall are presented in reference 7, but the technique is too complex for inclusion in a dynamic simulation.

When an airplane approaches the stall one well-known effect is an increase in maximum lift coefficient with increasing rate of change of angle of attack. Some studies of this effect are given in references 8 to 14. Selected data from these references are summarized in figure 7. Empirical methods used to predict the effect of rate of change of angle of attack on the maximum lift coefficient are given in references 15 and 16. These methods assume two-dimensional flow and require a knowledge of the static stall characteristics of the airfoil.

The data of figure 7 show wide differences in the magnitude of the effect of rate of change in angle of attack $\dot{\alpha}$ on the increase of maximum lift coefficient $C_{L,max}$. The magnitude of the effect depends on the configuration tested, airfoil section, Reynolds number, and Mach number. In cases for which a range of values of Mach number were covered in the reference reports, data are shown only at the lowest Mach number.

Mach number appears to have an important influence on the magnitude of the effect of $\dot{\alpha}$ on $C_{L,max}$. The effect is greatest at low Mach numbers, and decreases with increasing Mach number until it disappears at Mach numbers greater than 0.6. In reference 8, for example, the effect of $\dot{\alpha}$ is shown to increase all the way down to a Mach number of 0.1, the lowest value tested. An increase in the effect of $\dot{\alpha}$ also appears to be produced by increased Reynolds number, and by the use of airfoils with a high value of $C_{L,max}$ and a sharply peaked lift curve. In cases in which very small values of $\dot{\alpha}$ were tested, the value of $C_{L,max}$ first rose rapidly, but then appeared to increase linearly with further increases in $\dot{\alpha}$. At values of $\dot{\alpha}c/2V$ between 0.007 and 0.014 rad, which extend beyond the range shown in figure 7, the curves tended to level out. Those curves in figure 7 which do not extend to the origin represent test data in which sufficiently small values of $\dot{\alpha}$ were not included to determine the shape of the curve near the origin.

The data of reference 11, shown as a very short curve near the origin in figure 6, have the largest slope of $\Delta C_{L,max}$ vs $\dot{\alpha}$ of any of the curves shown. Despite the small range of $\dot{\alpha}$ covered, the number of test points taken within this range was large enough to define the curve adequately. The data were obtained in tests in the Langley full-scale tunnel of a parasol-winged light airplane, on which the wing leading edge had been especially smoothed for the tests. The high values of slope obtained in this test may perhaps be attributed to the low Mach number, relatively high Reynolds number, and lack of leading-edge disturbances.

The authors of reference 10 chose the relationship $\Delta C_{L,max} \approx 5\sqrt{\frac{\dot{\alpha}c}{2V}}$ ($\dot{\alpha}$ in rad/sec) as an empirical fit to data obtained in oscillating airfoil tests. This curve is plotted in figure 7. The test points on which the fit is based, however, are from values of $\dot{\alpha}c/2V$ of 0.004 to 0.010 rad. The curve, therefore, is not extended to the origin.

The dashed lines labeled "values used in simulation studies" are two curves which bracket most of the available experimental data. The upper curve is given by the formula

$$\Delta C_{L,max} = 6.325\sqrt{\frac{\dot{\alpha}c}{2V}}$$

and the lower curve is given by the formula

$$\Delta C_{L,max} = 20.0\,\frac{\dot{\alpha}c}{2V}$$

where $\dot{\alpha}$ is in rad/sec. These formulas are used to determine the stall point in subsequent simulation studies in this paper.

A representation of the dynamic stall behavior in a simulation must be capable of reproducing the forces and moments acting for arbitrary motions of the airplane. In general, because of the limited understanding of phenomena involving separated flow, the representation of the behavior is somewhat empirical and uncertain.

In the present study, a number of empirical formulations of the laws governing the forces and moments on the wing are tried. The formulations are limited to those which can be represented conveniently on the hybrid computer. No attempt is made to provide a physical simulation of actual flow phenomena. Comparison of the resulting dynamic behavior with measured airplane motions serves as a guide to judge which of the formulations may be more realistic. A description of each of the assumed representations of the force and moment characteristics is given with the corresponding airplane motions in the following section.

RESULTS

Motion in Unstalled Condition

As a check on the validity of the analog portion of the simulation, records of the response of the simulated airplane to a step deflection of the elevator were obtained from the analog computer. For these runs, the variations with angle of attack of the lift, drag, and pitching-moment coefficients are those given previously in the section entitled "Equations Used in Simulation." Time histories of the resulting response, which show primarily the phugoid motion at two values of airspeed, are shown in figure 8. The fact that the period and damping of the phugoid motion agrees with values predicted analytically for these cases provides a partial check on the validity of the analog simulation. Because the lift and pitching-moment curves remain linear indefinitely, no evidence of stall in terms of uncommanded motions can be obtained from this simulation.

Stall Based on Static Aerodynamic Characteristics

The values of lift, drag, and pitching-moment coefficients for the wing-fuselage combination as a function of angle of attack which were assumed to represent the static aerodynamic characteristics are shown in figure 9(a). The pitching moments are given about an assumed center-of-gravity location of 0.25c. Beyond the stall, the center of pressure on an unswept wing moves to 0.50c, which would give a value of C_m of -0.25 for a value of C_L of 1.0. For a typical wing-fuselage combination, however, the center of pressure is somewhat further forward. The assumption is made that the center of pressure beyond the stall is at 0.40c, resulting in a value of C_m of -0.15. The response of the simulated airplane to a ramp input of the elevator with a rate of 0.016 rad/sec (0.917 deg/sec) starting from a trim condition slightly below the stall is shown in figure 9(b). Note the expanded time scale of these figures as compared to those of figure 8. In figure 9 and subsequent figures, the values of C_L, C_D, and C_m shown on the time histories are those of the wing-fuselage combination. The airplane exhibits a very small amplitude short-period pitching oscillation which builds up to a constant amplitude in the region beyond the stall break. This oscillation may be attributed to the negative lift-curve slope in this region, inasmuch as the damping of the short-period motion depends on the pitch damping derivatives plus a term proportional to C_{L_α}. When the angle of attack increases to the point where the lift curve is horizontal, the oscillation disappears.

Stall Based on Static Lift Curve With Abrupt Break

Subsequent cases which model hysteresis in the aerodynamic forces include an abrupt break in the lift and pitching-moment curves at the stall. For comparison, a case using static aerodynamic characteristics with abrupt breaks is included. These

characteristics are shown in figure 10(a), and the time history of the resulting stall motion is shown in figure 10(b). The abrupt breaks in lift and pitching-moment coefficients result in a motion typical of limit cycle with a period of about 9/10 sec and an amplitude much larger than that of the preceding case. (See fig. 9(b).) The oscillation disappears when the angle of attack at the minimum point of the oscillation increases to a point beyond the break. This example shows that an abrupt break in the lift and pitching-moment characteristics, even without hysteresis, can theoretically lead to longitudinal oscillations.

Dynamic Stall With Hysteresis in Lift, Drag, and Moment Curves – Condition 1

In this condition, an attempt is made to simulate dynamic stall characteristics, such as those shown in figure 6, by incorporating hysteresis in the curves of lift, drag, and pitching-moment coefficients as a function of angle of attack. The assumed aerodynamic characteristics are shown in figure 11(a). The static lift curve is the same as that used in figure 10(a). However, if the angle of attack is increasing, the angle of attack at the stall is increased by an amount corresponding to the upper curve of figure 7. The function defining the stall point is

$$\Delta C_{L,max} = 6.325\sqrt{\frac{\dot{\alpha}c}{2V}}$$

where $\dot{\alpha}$ is in rad/sec. For use in the simulation, this formula is converted to an expression for the stall angle of attack by the following procedure:

$$\alpha_{stall} = 0.258 + \frac{6.325}{C_{L_\alpha}}\sqrt{\frac{c}{2V}}\sqrt{\dot{\alpha}}$$

$$= 0.258 + \frac{6.325}{5.02}\sqrt{\frac{1.338}{2(29.1)}}\sqrt{\dot{\alpha}}$$

$$= 0.258 + 0.191\sqrt{\dot{\alpha}}$$

The airspeed, 29.1 m/sec, corresponds to flight at a value of C_L of 1.295. The stall point given by this function corresponds to the upper curve of figure 7. As an example of the effect of $\dot{\alpha}$ given by this formula, a value of $\dot{\alpha}$ of 1 deg/sec raises the stall angle by 1.446^o. Another feature of the characteristics given in figure 11(a) is that once the

wing is stalled the lift coefficient remains on the flat or stalled part of the curve until the angle of attack decreases below the point where this flat curve intersects the linear lift curve. The drag and pitching-moment coefficients also stay on the stalled curves until the angle of attack has been reduced to this point. Thus, if the angle of attack starts to increase again before it has dropped to the unstalled condition, the wing remains stalled and no further hysteresis loops are encountered. The characteristics resulting from these assumptions are shown in figure 11(b). The airplane exhibits an abrupt nose-down motion at the stall, but the resulting oscillation damps out rapidly and does not reappear while the airplane remains in the stalled region. Some runs in this condition with a lower rate of increase of elevator angle showed multiple oscillations as the coefficients went around the hysteresis loops because the angle of attack during the oscillation decreased below the assumed unstalled value ($\alpha = 0.203$ rad).

Dynamic Stall With Hysteresis – Condition 2

This condition differs from condition 1 in that if the airplane is in a stalled condition and the angle of attack starts to increase, the coefficients will return to their unstalled values, provided the angle of attack is less than the static stall point, $\alpha = 0.258$ rad. The assumed characteristics are shown in figure 12. As the angle of attack increases, the airplane remains unstalled so long as the angle of attack is below that given by the dynamic stall condition, namely:

$$\alpha_{stall} = 0.258 + 0.191\sqrt{\dot{\alpha}}$$

where α is in rad. The stall behavior under these conditions is shown in figure 12(b). Upon reaching the stall, the airplane performs several cycles of oscillation with a period of about 2 sec.

Dynamic Stall With Hysteresis – Condition 3

The dynamic stall characteristics for this condition are the same as those for condition 2 except that the effect of $\dot{\alpha}$ on $C_{L,max}$ is less, and α_{stall} is a linear function $\dot{\alpha}$ instead of a square root function of this quantity. The angle of attack at the stall break corresponds to the lower curve of figure 7 and is given by the equation: $\alpha_{stall} = 0.258 + 0.0915\dot{\alpha}$. As an example of the effect of $\dot{\alpha}$ given by the formula, a value of $\dot{\alpha}$ of 1 deg/sec raises the stall angle by 0.091^{o}. The resulting motion is shown in figure 13. The main difference from the preceding case (condition 2) is a shorter period of the limit cycle oscillation because in each oscillation the angle of attack does not increase to such a large value before the stall occurs.

Effect of Lag of Downwash

Incorporating lag in the downwash, as described in the section on equations of motion, involved a certain amount of complication in the programming of the hybrid computer. In order to determine whether this complication was warranted, a repeat of the case shown in figure 12(b) was made with the lag of downwash eliminated. In this case downwash is simply proportional to the instantaneous value of lift coefficient with no lag in its effect at the tail. The results are shown in figure 14. The motion is only very slightly different from that of figure 12(b). It can be concluded from this figure that the effect of downwash lag on the motion at the stall is small.

The assumption that the downwash is proportional to the lift coefficient, however, may not be very realistic. In practice, for certain configurations, both the wing wake and the associated downwash may affect the tail more severely than assumed in the present paper. If the wing stalls first at the root, the loss of lift over the inboard sections may cause a rapid reduction in downwash at the stall. Furthermore, the downwash may undergo large transient variations as a result of vortices shed from the wing as it goes into and out of the stalled region. To study these phenomena, it would be desirable to conduct dynamic wind-tunnel tests of complete models.

DISCUSSION

Comparison of the results shown in figure 1 and in figures 12(b) and 13 illustrates that hysteresis in the lift and pitching-moment curves can result in motion which resembles the longitudinal oscillation encountered by airplanes at the stall. The case shown in figure 10(b), in which the aerodynamic characteristics have an abrupt break at the stall, produces an oscillation typical of a limit cycle, but this oscillation is of a higher frequency than that exhibited in flight. Also, the abrupt stall break is not considered to be realistic for a complete airplane with initial stall at the root sections because it would require simultaneous stall of the flow from the leading edge across the entire span. The presence of the abrupt break which was used as a part of the hysteresis model, however, may have some effect on the nature of the oscillations obtained in the cases with hysteresis. The sharp corners and abrupt changes in values of lift and pitching moment in going around the hysteresis loop probably are responsible for the shape of the wave form of the oscillation obtained in the simulation, which differs from the more nearly sinusoidal wave form obtained in flight.

Comparison of the data in figures 11(b) and 12(b) shows that in the simulation studies the aerodynamic force and pitching moment must continue to exhibit a hysteresis loop during successive cycles of motion if the oscillation is to continue. In the case of figure 11(b) the aerodynamic force and pitching moment remain constant after the first

hysteresis loop is encircled because the angle of attack remains above the point where the flow was assumed to be completely stalled. Tests of oscillating airfoils have shown that during the course of an oscillation, the lift and pitching moment exhibit hysteresis loops even though the angle of attack may always be above that required for the static stall (ref. 6). The hysteresis condition 2 (fig. 12) is therefore considered to be a more realistic representation of the actual dynamic stall characteristics.

Comparison of conditions 2 and 3 (figs. 12 and 13) shows that the period of the longitudinal oscillation at the stall is dependent on the effect of the rate of change of angle of attack $\dot{\alpha}$ on the maximum lift coefficient. The two conditions used (conditions 2 and 3) may be expected to bracket the actual effect of $\dot{\alpha}$ on the maximum lift coefficient. Correlation of wind-tunnel data, as discussed in reference 15, indicates that airfoils which have a high maximum lift coefficient and subsequent flow separation from the leading edge may be expected to have a large effect of $\dot{\alpha}$ on the maximum lift coefficient. By similar reasoning, it might be expected that a high Reynolds number such as occurs in flight would result in a greater effect of $\dot{\alpha}$ on the maximum lift coefficient than is measured in model tests at low Reynolds numbers. Comparison of the period of the oscillation measured in flight (fig. 1) with the simulator results indicates that the flight data are closer to the assumption of condition 2, in which $\dot{\alpha}$ has a large effect on the stall angle.

Comparison of figures 12(b) and 14, which differ only in that the lag of downwash was omitted in figure 14, shows that the lag of downwash is relatively unimportant in determining the stall behavior. The lack of importance of this lag might be expected because the maximum value of the lag, even at the stall speed, is only 1/10 sec. As mentioned previously, however, the law governing the variation of downwash with lift coefficient may be a factor of importance in determining the stall characteristics. In the present study the hysteresis effect on the pitching moment was assumed to be applied primarily to the moments acting on the wing. Data given in the reference reports (for example, ref. 7) show that the large negative pitching moment which occurs following the stall break is caused by the vortex shed from the leading edge of the wing passing close to the trailing edge and inducing a negative pressure in this region immediately following the dynamic stall. The value of this negative pitching moment for the wing-fuselage combination, $C_m = -0.15$, is consistent with the values frequently measured in tests on two-dimensional airfoils. In the case of the complete airplane, however, if the stall only occurred in the region of the wing root, the wing contribution would be expected to be less than this value. On the other hand, the effect of loss of downwash at the tail would contribute to the negative pitching moment of the complete configuration. Thus, in the present simulation study, the value of C_m of -0.15 which is reached following the stall might be considered as an approximation to the combined effects of wing pitching moments and effects of downwash changes on the tail for the entire airplane. Further wind-tunnel studies to determine

the dynamic stall characteristics of complete configurations are required to obtain the nature of hysteresis loops for the complete configuration and to determine the relative magnitudes of the contributions of the wing and the horizontal tail to the dynamic pitching moments.

The flight data shown for several types of airplanes indicate that the longitudinal oscillation at the stall is a fairly common phenomenon and is not restricted to any particular configuration. If the rapid roll motion at the stall typical of many airplanes were prevented, the longitudinal oscillation would probably appear still more frequently. The differences in period of the oscillation with flap up and flap down, shown in figures 2(a) and 2(b), may indicate a larger effect of rate of change of angle of attack on maximum lift coefficient with flap down than with flap up though many other differences in the stall phenomena with flap down may also be involved. No wind-tunnel measurements appear to be available on dynamic stall effects on flapped airfoils. Such wind-tunnel tests both for flapped airfoils and for complete airplane configurations would be of interest to provide a more complete explanation of the oscillations investigated in this report.

CONCLUDING REMARKS

Hybrid simulation studies of the longitudinal motion of a straight-wing airplane at the stall have shown that short-period longitudinal oscillations, which are sometimes observed in actual stall tests, can be simulated by modeling the hysteresis in the development of lift and pitching moments on the wing as a function of angle of attack. Because of the lack of dynamic stall data for the complete airplane configurations, the studies presented in this report are exploratory in nature. Complete data on the dynamic stall characteristics of an actual configuration would be required to make a more accurate estimate of the longitudinal behavior at the stall.

Langley Research Center
National Aeronautics and Space Administration
Hampton, VA 23665
June 13, 1978

REFERENCES

1. Crane, H. L.; Talmage, D. B.; and Gray, W. E., Jr.: Measurement of Flying Qualities of a De Havilland Mosquito F88 Airplane (AAF No. 43-334960). II.- Longitudinal Stability and Control Characteristics. NACA WR L-614, 1945. (Formerly NACA MR L5G11.)

2. Hunter, P. A.; and Vensel, J. R.: A Flight Investigation To Increase the Safety of a Light Airplane. NACA TN 1203, 1947.

3. Huston, Wilber B.; and Skopinski, T. H.: Measurement and Analysis of Wing and Tail Buffeting Loads on a Fighter Airplane. NACA Rep. 1219, 1955. (Supersedes NACA TN 3080.)

4. Windsor, Richard I.: Measurement of Aerodynamic Forces on an Oscillating Airfoil. USAAVLABS Tech. Rep. 69-98, U.S. Army, Mar. 1970. (Available from DDC as AD 873 253.)

5. McCroskey, W. J.: Some Current Research In Unsteady Fluid Dynamics – The 1976 Freeman Scholar Lecture. ASME, Ser. I: Fluids Eng., vol. 99, no. 1, Mar. 1977, pp. 8-38.

6. Liiva, Jaan; Davenport, Franklyn J.; Gray, Lewis; and Walton, Ivor C.: Two-Dimensional Tests of Airfoils Oscillating Near Stall. Volume 1 – Summary and Evaluation of Results. USAAVLABS Tech. Rep. 68-13A, U.S. Army, Apr. 1968. (Available from DDC as AD 670 959.)

7. Ham, Norman D.: Aerodynamic Loading on a Two-Dimensional Airfoil During Dynamic Stall. AIAA J., vol. 6, no. 10, Oct. 1968, pp. 1927-1934.

8. Harper, Paul W.; and Flanigan, Roy E.: The Effect of Rate of Change of Angle of Attack on the Maximum Lift of a Small Model. NACA TN 2061, 1950.

9. Conner, Fox; Willey, Craig; and Twomey, William: A Flight and Wind Tunnel Investigation of the Effect of Angle-of-Attack Rate on Maximum Lift Coefficient. NASA CR-231, 1965.

10. Fukushima, T.; and Dadone, L. U.: Comparison of Dynamic Stall Phenomena for Pitching and Vertical Translation Motions. NASA CR-2793, 1977.

11. Silverstein, Abe; Katzoff, S.; and Hootman, James A.: Comparative Flight and Full-Scale Wind-Tunnel Measurements of the Maximum Lift of an Airplane. NACA Rep. 618, 1938.

12. Davis, Don D., Jr.; and Sweberg, Harold H.: Investigation of Some Factors Affecting Comparisons of Wind-Tunnel and Flight Measurements of Maximum Lift Coefficients for a Fighter-Type Airplane. NACA TN 1639, 1948.

13. Spreiter, John R.; Galster, George M.; and Blair, William K.: Effect of Mach and Reynolds Numbers on the Maximum Lift Coefficient Obtainable in Gradual and Abrupt Stalls of a Pursuit Airplane Equipped With a Low-Drag Wing. NACA WR A-5, Bur. Aero., 1945.

14. Gadeburg, Burnett L.: The Effect of Rate of Change of Angle of Attack on the Maximum Lift Coefficient of a Pursuit Airplane. NASA TN 2525, 1951.

15. Ericsson, Lars E.; and Reding, J. Peter: Dynamic Stall Analysis in Light of Recent Numerical and Experimental Results. J. Aircr., vol. 13, no. 4, Apr. 1976, pp. 248-255.

16. Ericsson, Lars E.; and Reding, J. Peter: Further Consideration of "Spilled" Leading-Edge Vortex Effects on Dynamic Stall. J. Aircr., vol. 14, no. 6, June 1977, pp. 601-603.

TABLE I.- CHARACTERISTICS OF AIRPLANE AND FLIGHT CONDITIONS USED IN SIMULATION

W, N	9015.7
m, kg	919.35
S, m^2	13.378
c, m	1.338
I_Y, kg-m^2	1801
l_t, m	4.556
S_t, m^2	2.508
S_t/S	0.1875
l_t/c	3.405
ρ, kg/m^3	1.2266
$P_m\eta$, kW	119.3
g, m/sec^2	9.8066
$C_{L_{\alpha,w}}$, per rad	5.02
$C_{L_{\alpha,t}}$, per rad	4.03
$\partial\epsilon/\partial\alpha$	0.4
τ	0.5
$C_{D,o}$	0.03
$C_{D_{\alpha^2}}$, per rad^2	1.07
x_o/c	0.18
x/c	0.25

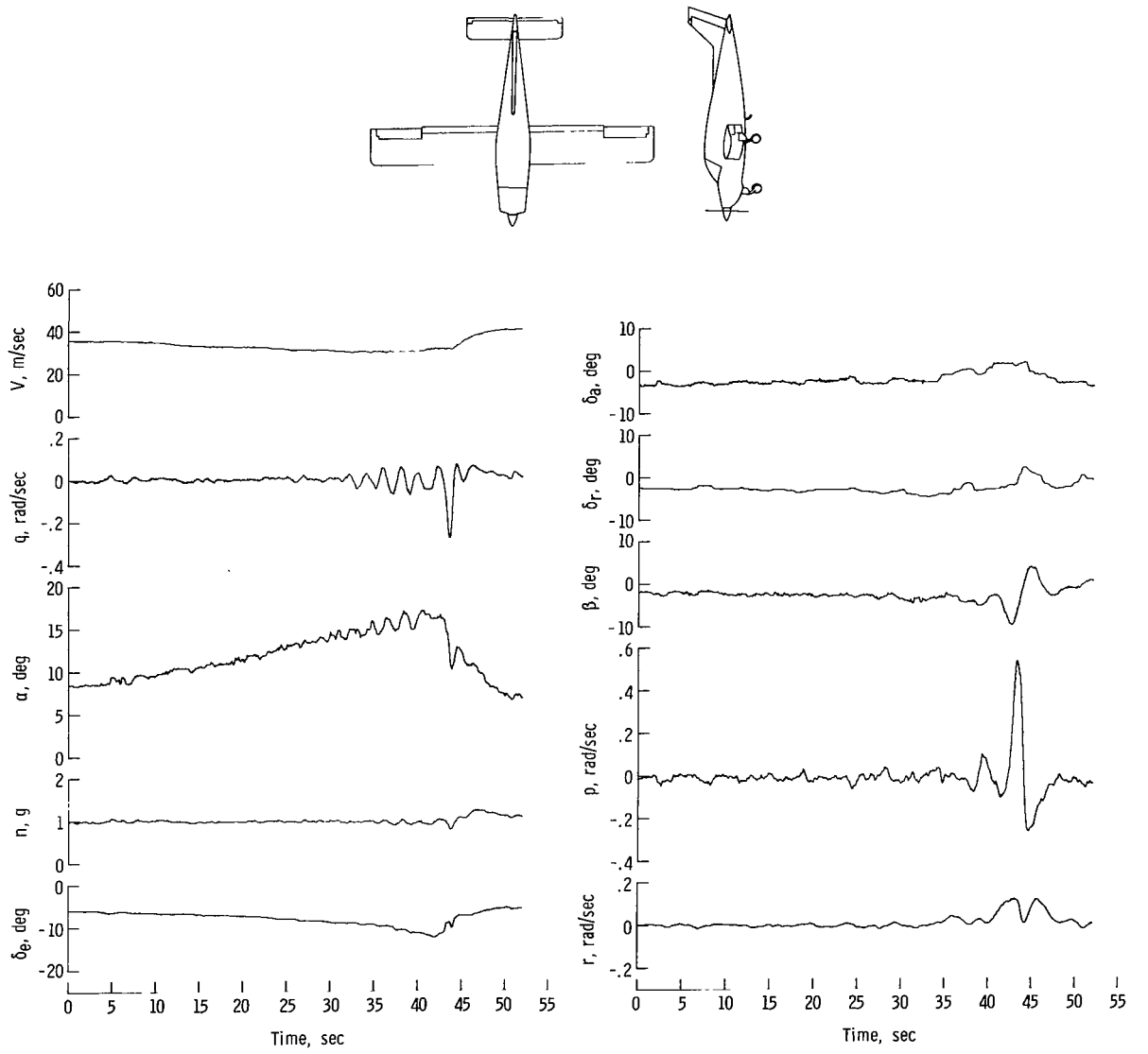

Figure 1.- Time history of stall of a low-wing general-aviation airplane in the power-off, flap-up condition.

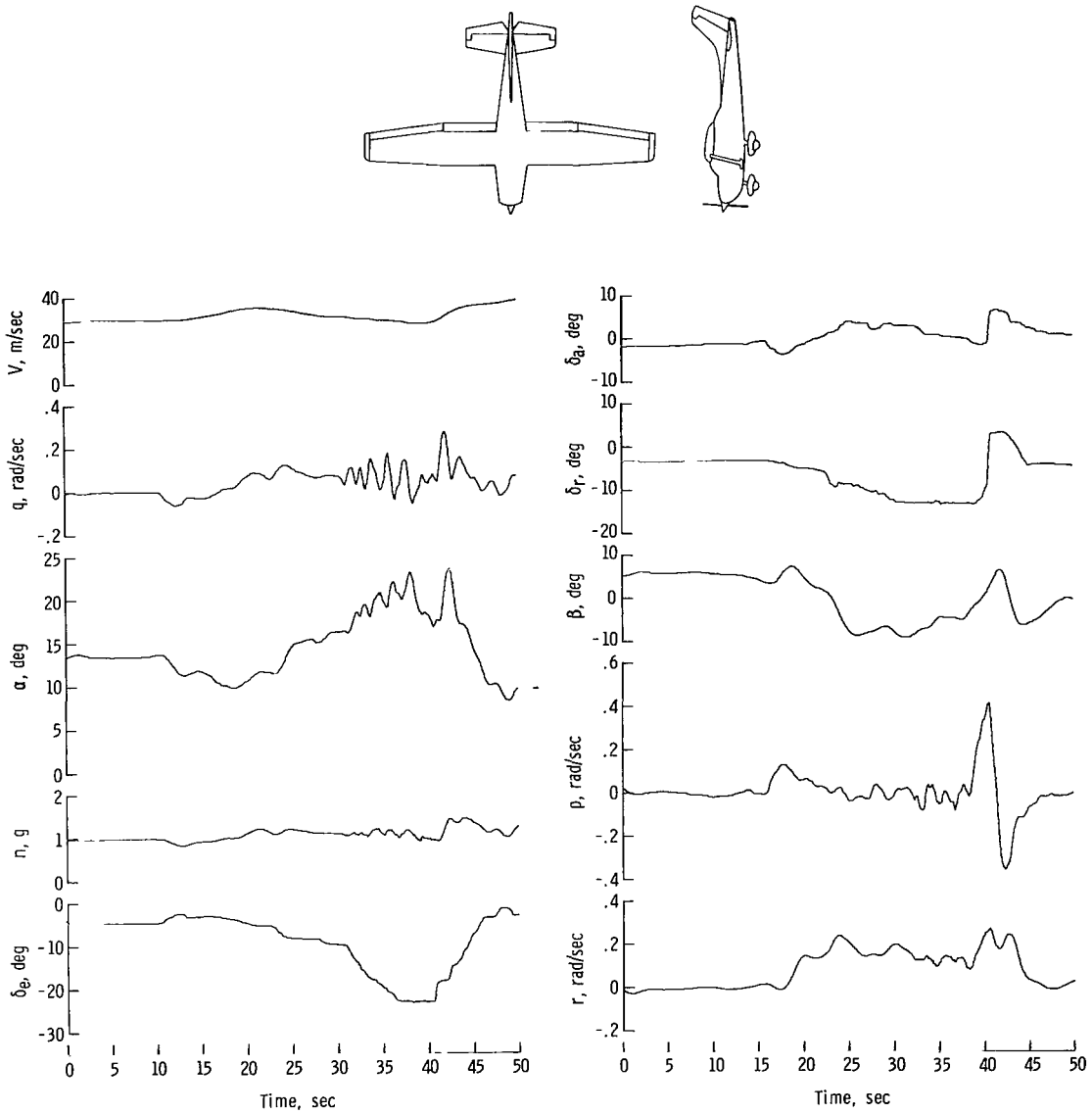

(a) Flap up.

Figure 2.- Time histories of stall of a high-wing general-aviation airplane in the power-off condition.

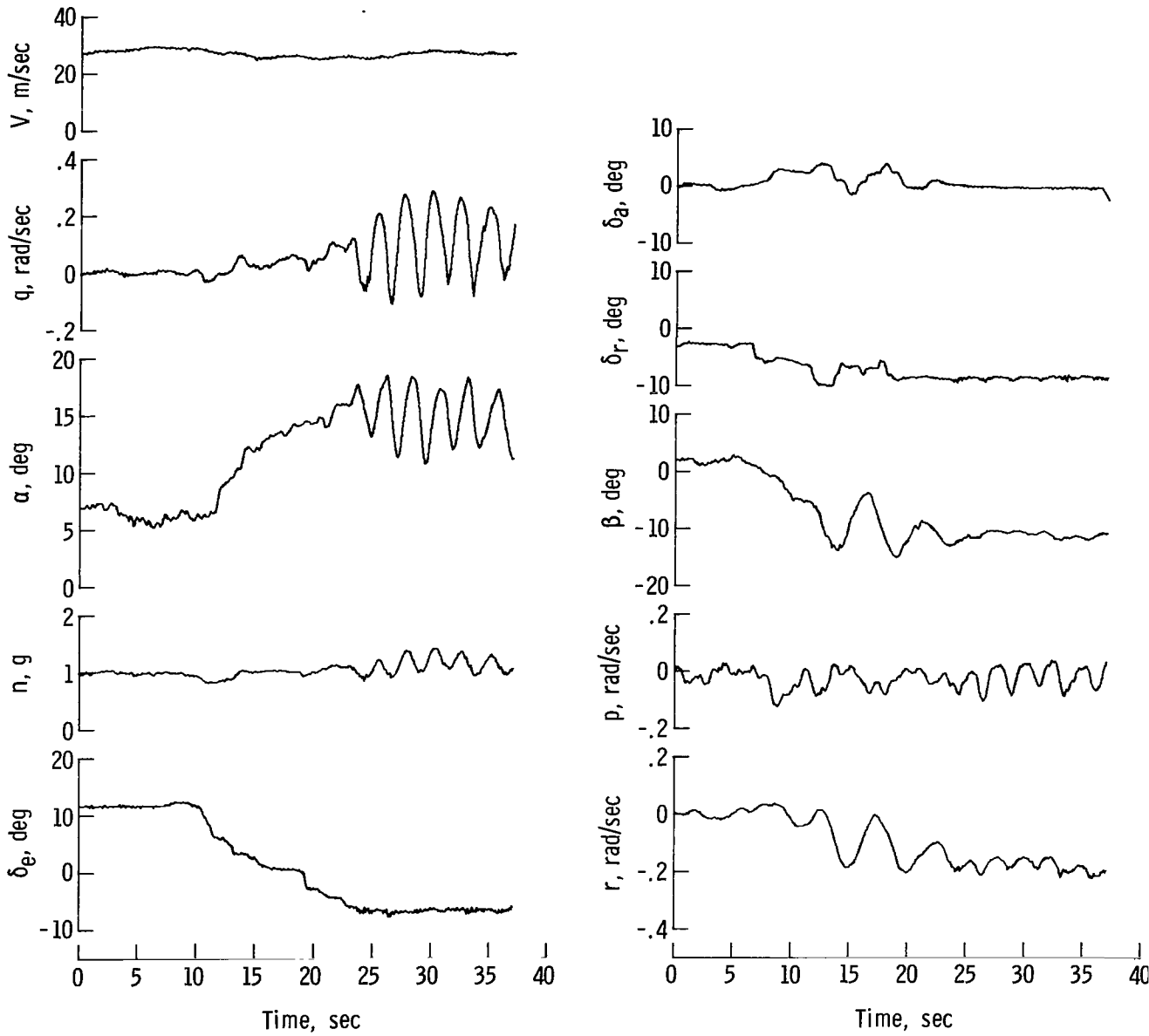

(b) Flap down.

Figure 2.- Concluded.

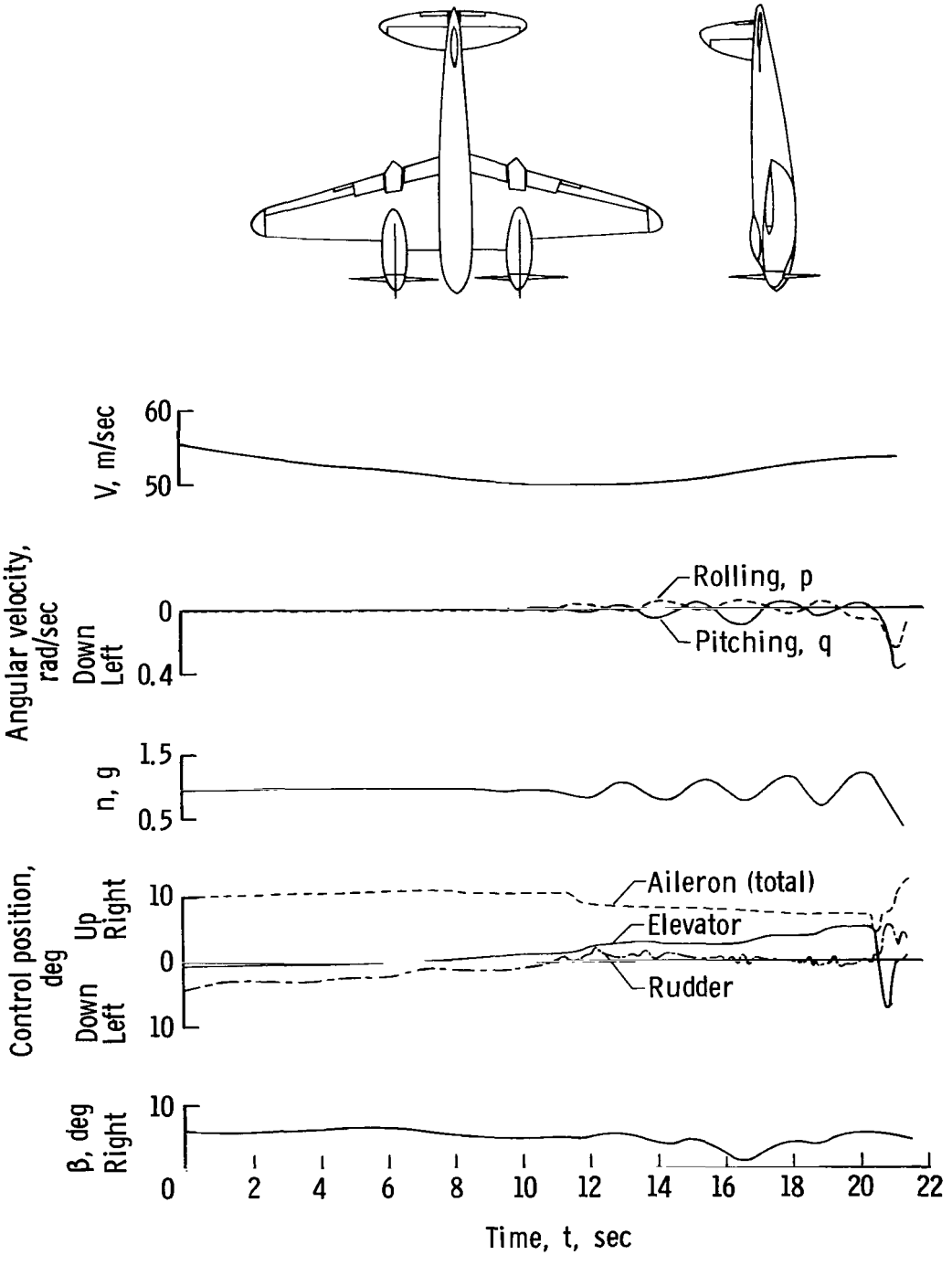

Figure 3.- Time history of stall of a twin-engine light bomber airplane in the power-off, flap-up condition.

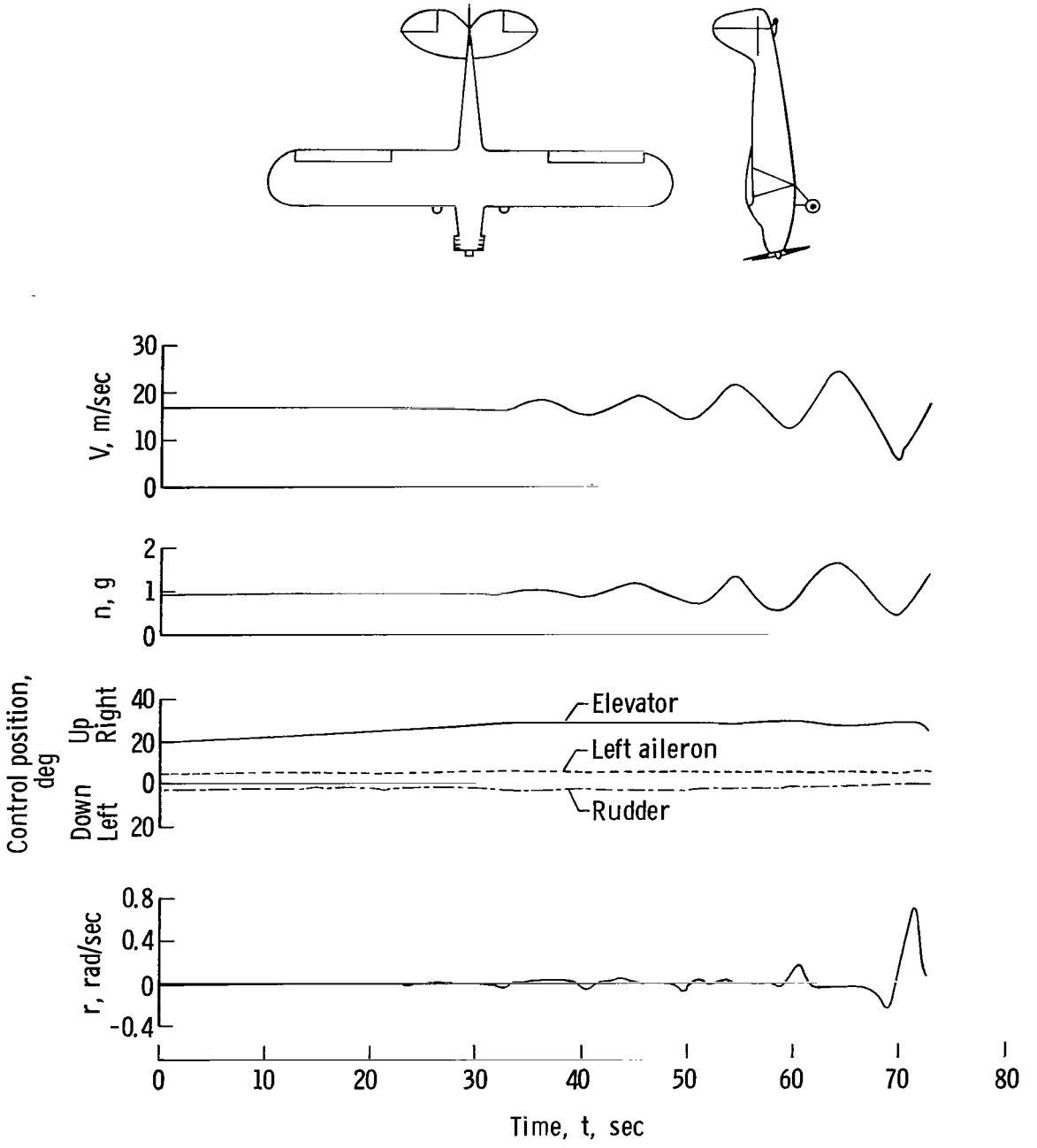

Figure 4.- Time history of stall of a light airplane with modifications to improve stalling characteristics.

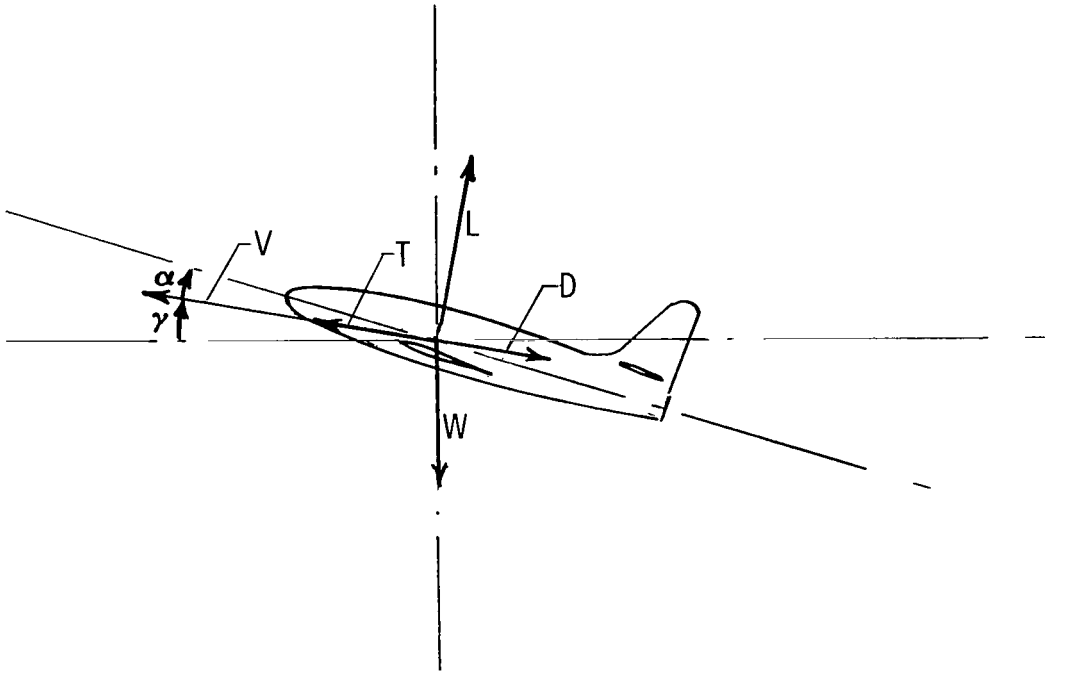

Figure 5.- System of axes used in analysis.

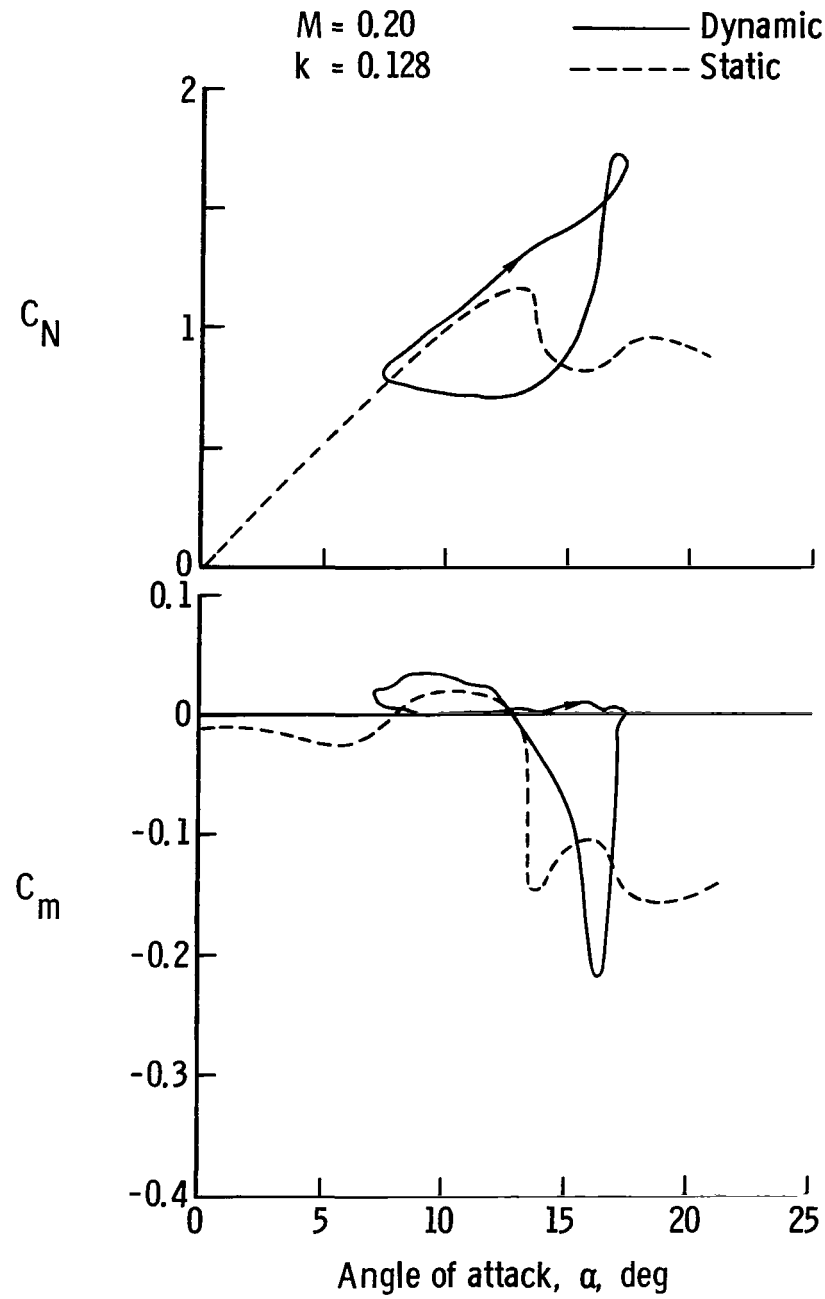

(a) Data from reference 4. NACA 0012 airfoil; $R \approx 2.6 \times 10^6$.

Figure 6.- Typical variations of normal-force coefficient and pitching-moment coefficient with angle of attack during sinusoidal pitching oscillations in the neighborhood of the stall.

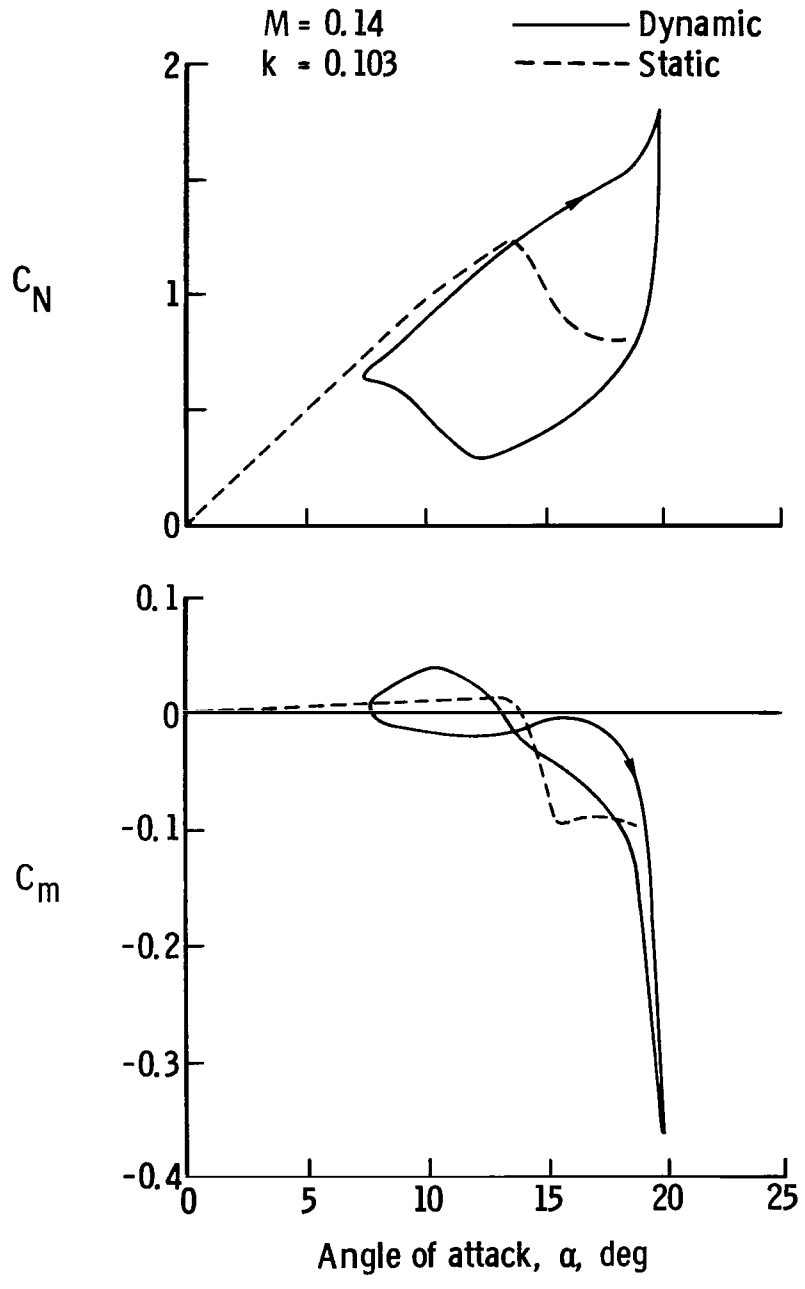

(b) Data from reference 6. NACA 0012 airfoil; $R \approx 0.93 \times 10^6$.

Figure 6.- Continued.

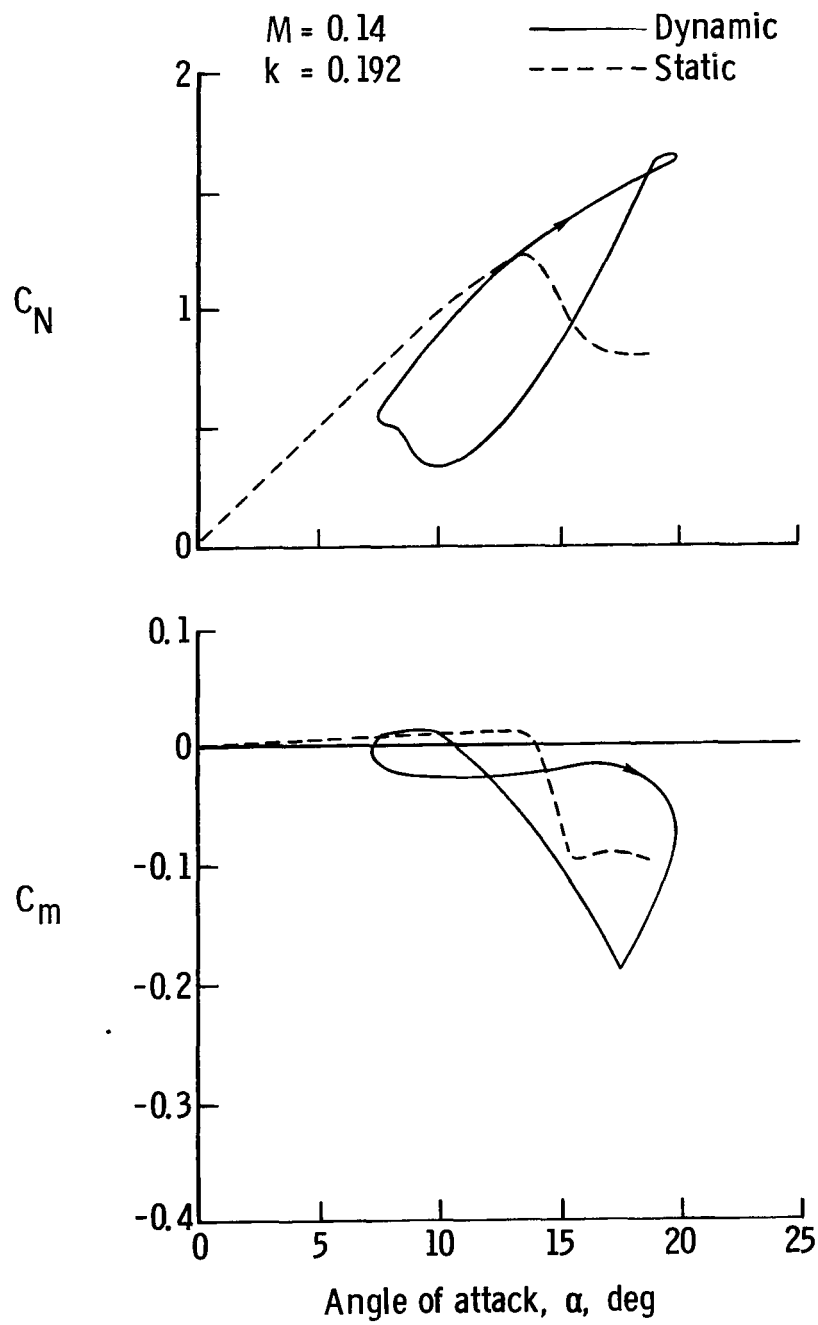

(c) Data from reference 6. NACA 0012 airfoil; $R \approx 0.93 \times 10^6$.

Figure 6.- Concluded.

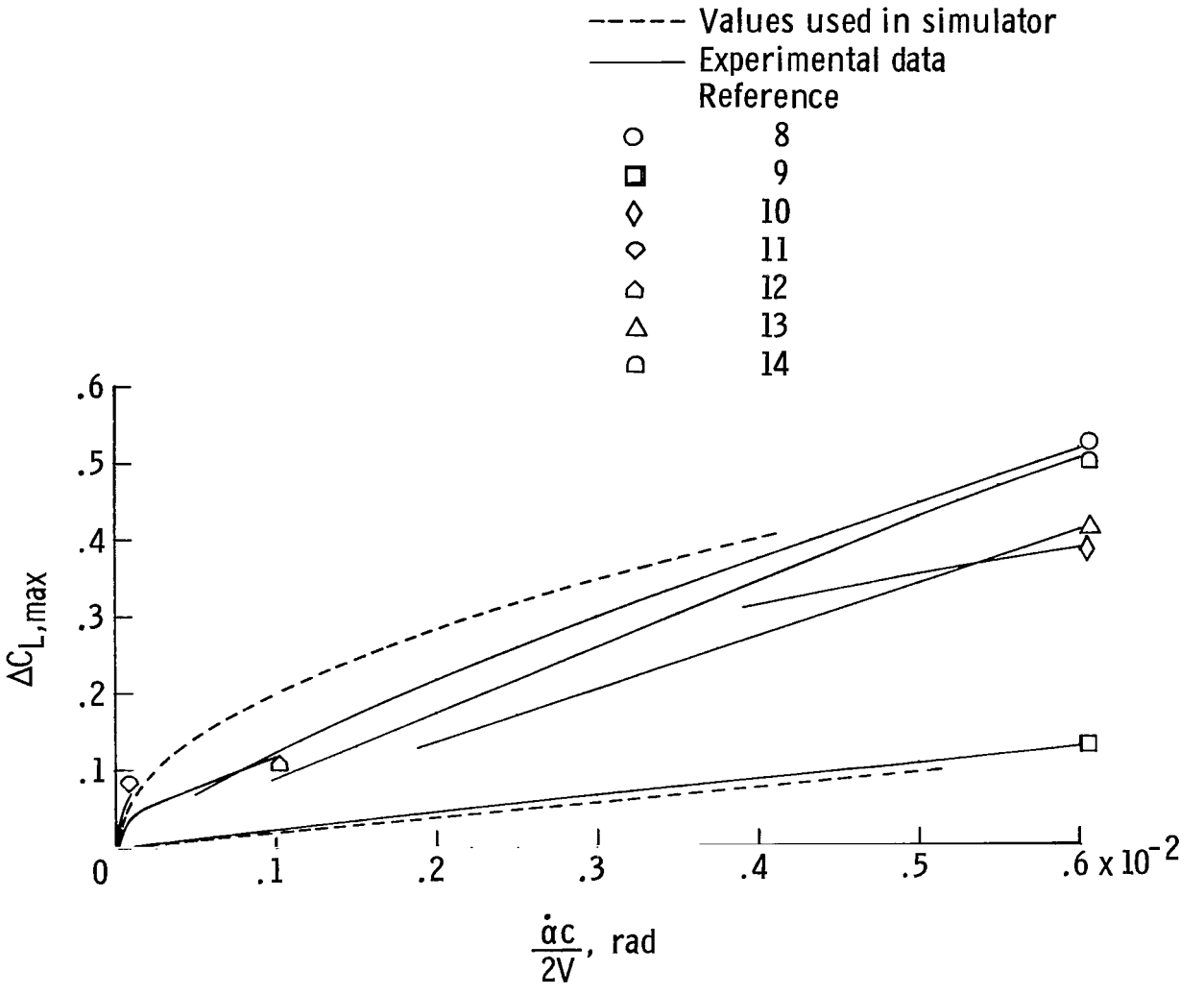

Figure 7.- Effect of rate of change of angle of attack on change in maximum lift coefficient.

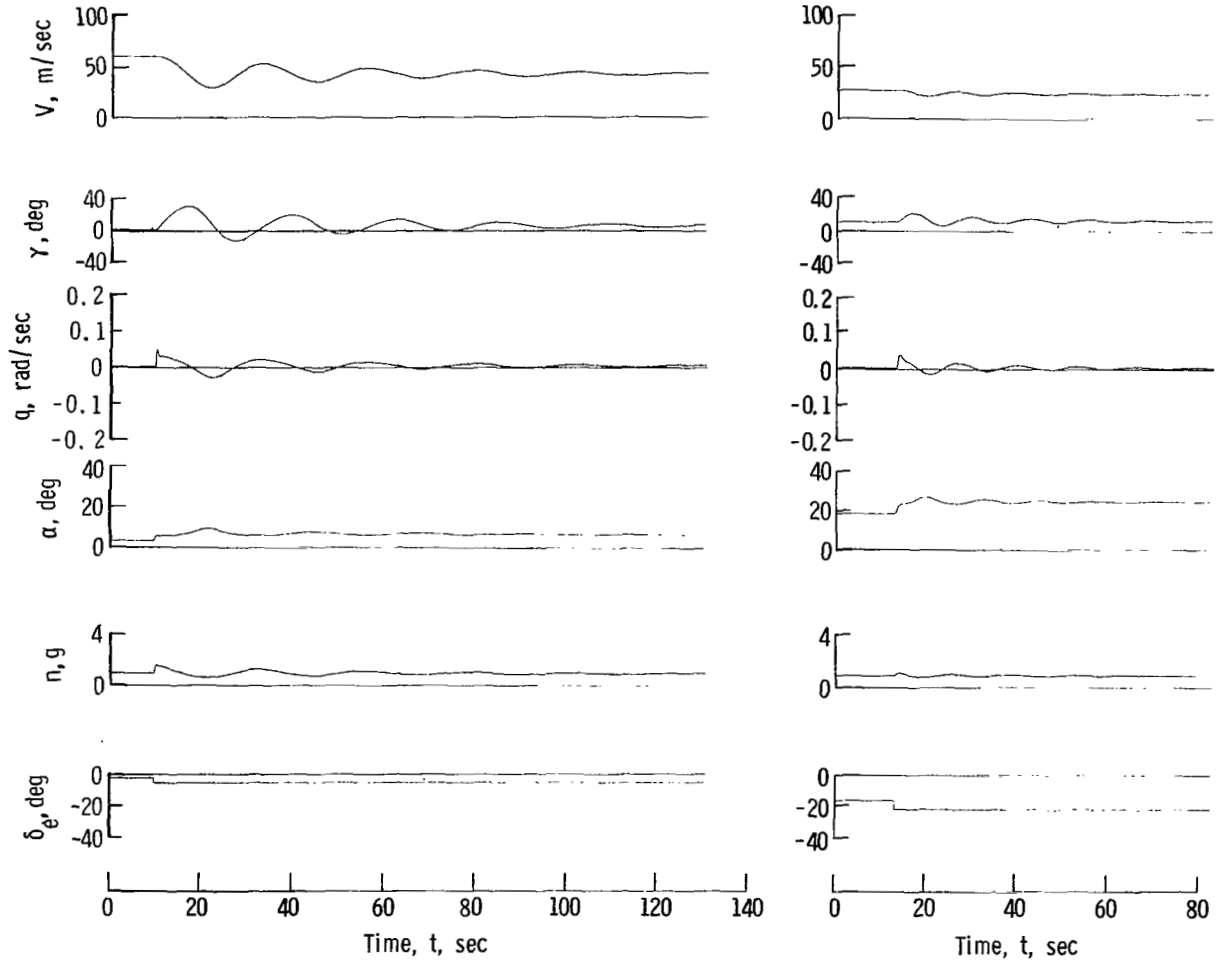

(a) Airspeed, 59.2 m/sec.

(b) Airspeed, 26.6 m/sec.

Figure 8.- Time histories of response to step input of the elevator at two values of airspeed, unstalled aerodynamic characteristics.

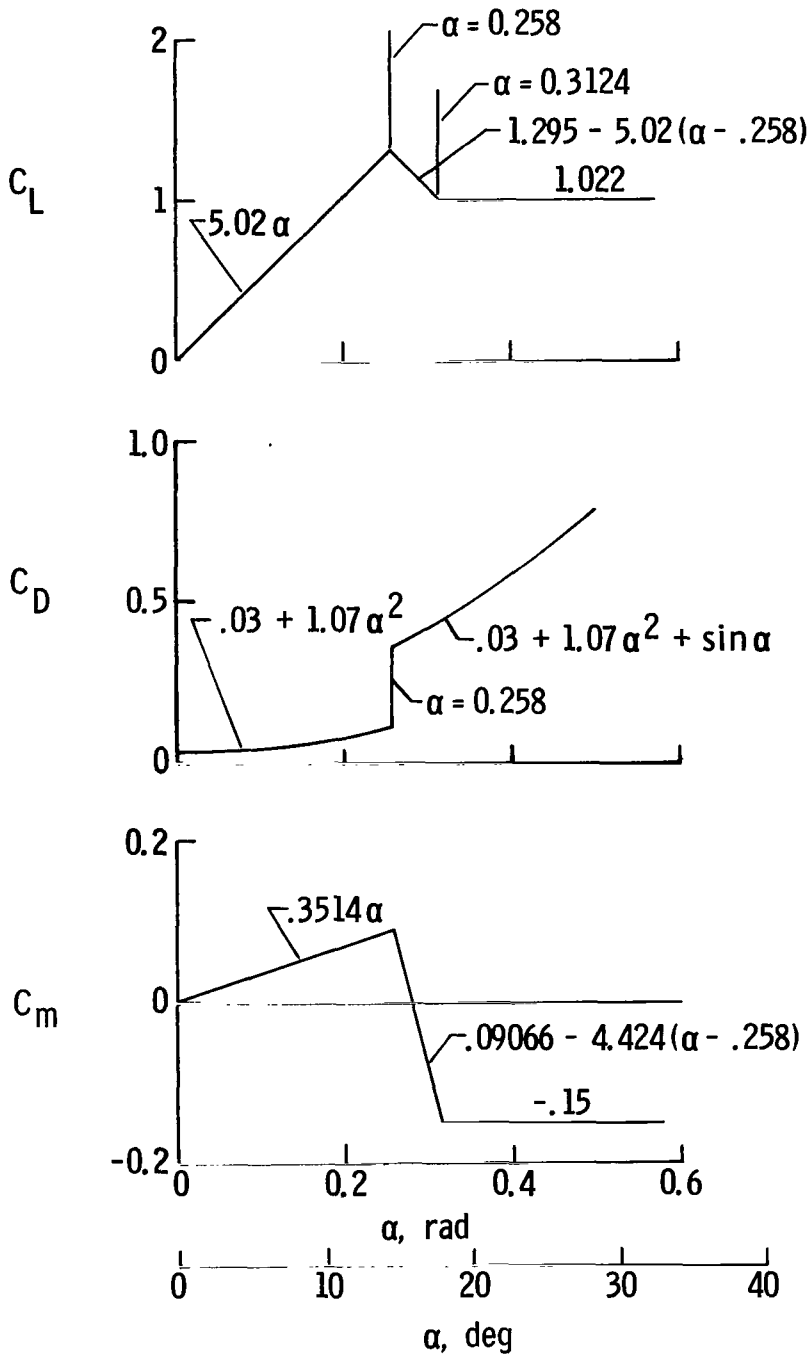

(a) Assumed static aerodynamic characteristics.

Figure 9.- Stall with static aerodynamic characteristics.

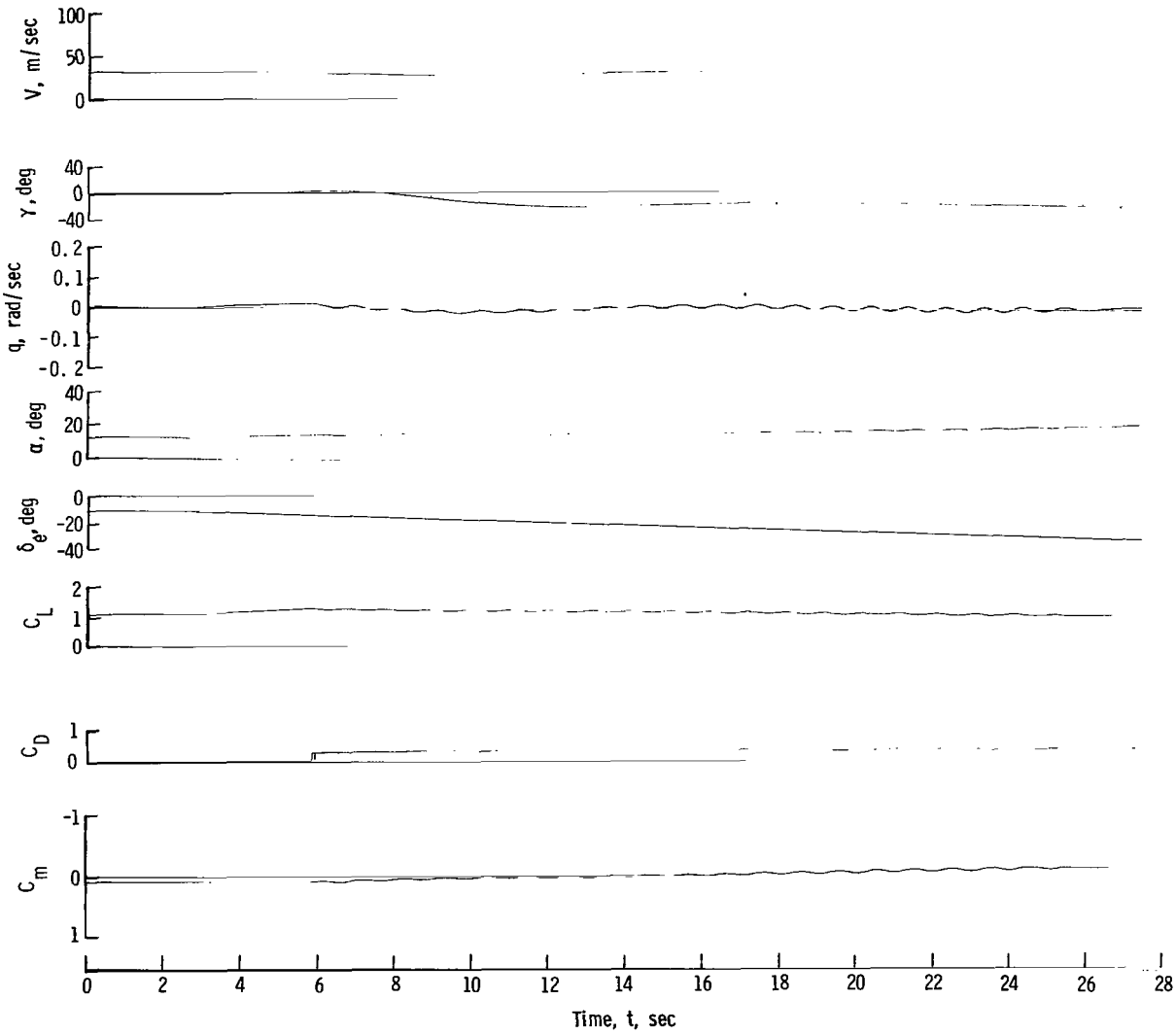

(b) Time history of stall with slow ramp input of elevator, static aerodynamic characteristics.

Figure 9.- Concluded.

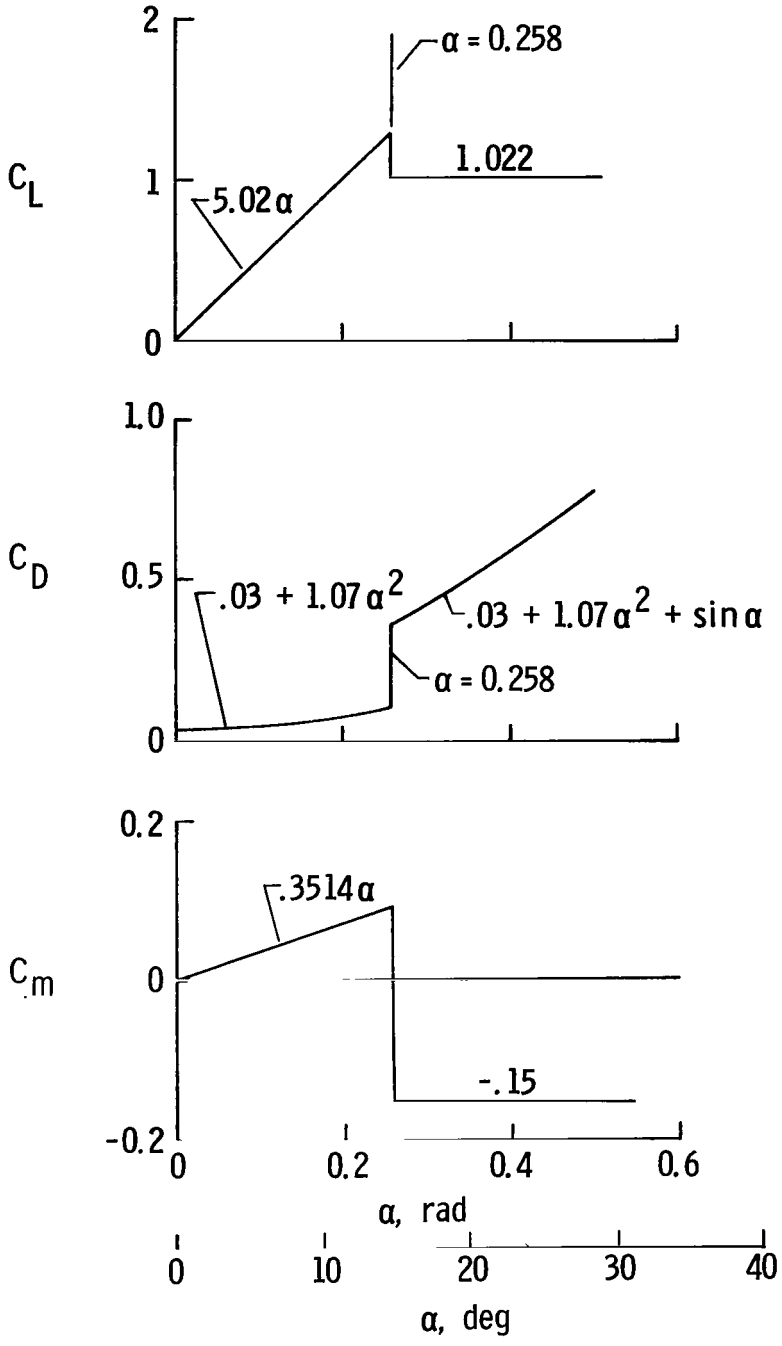

(a) Assumed static aerodynamic characteristics with abrupt break.

Figure 10.- Stall with static aerodynamic characteristics having abrupt break.

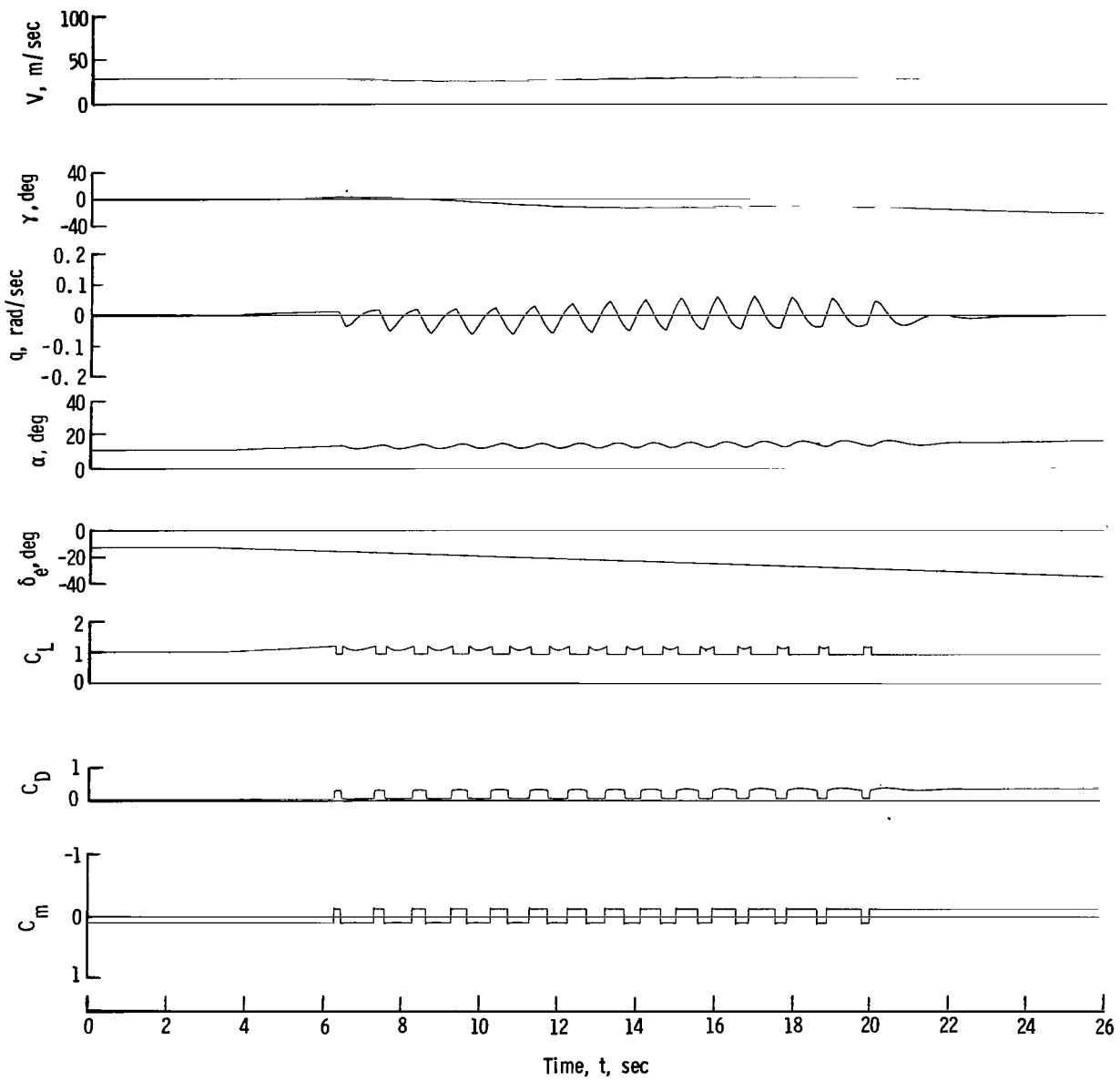

(b) Time history of stall with slow ramp input of elevator, static aerodynamic characteristics having abrupt break.

Figure 10.- Concluded.

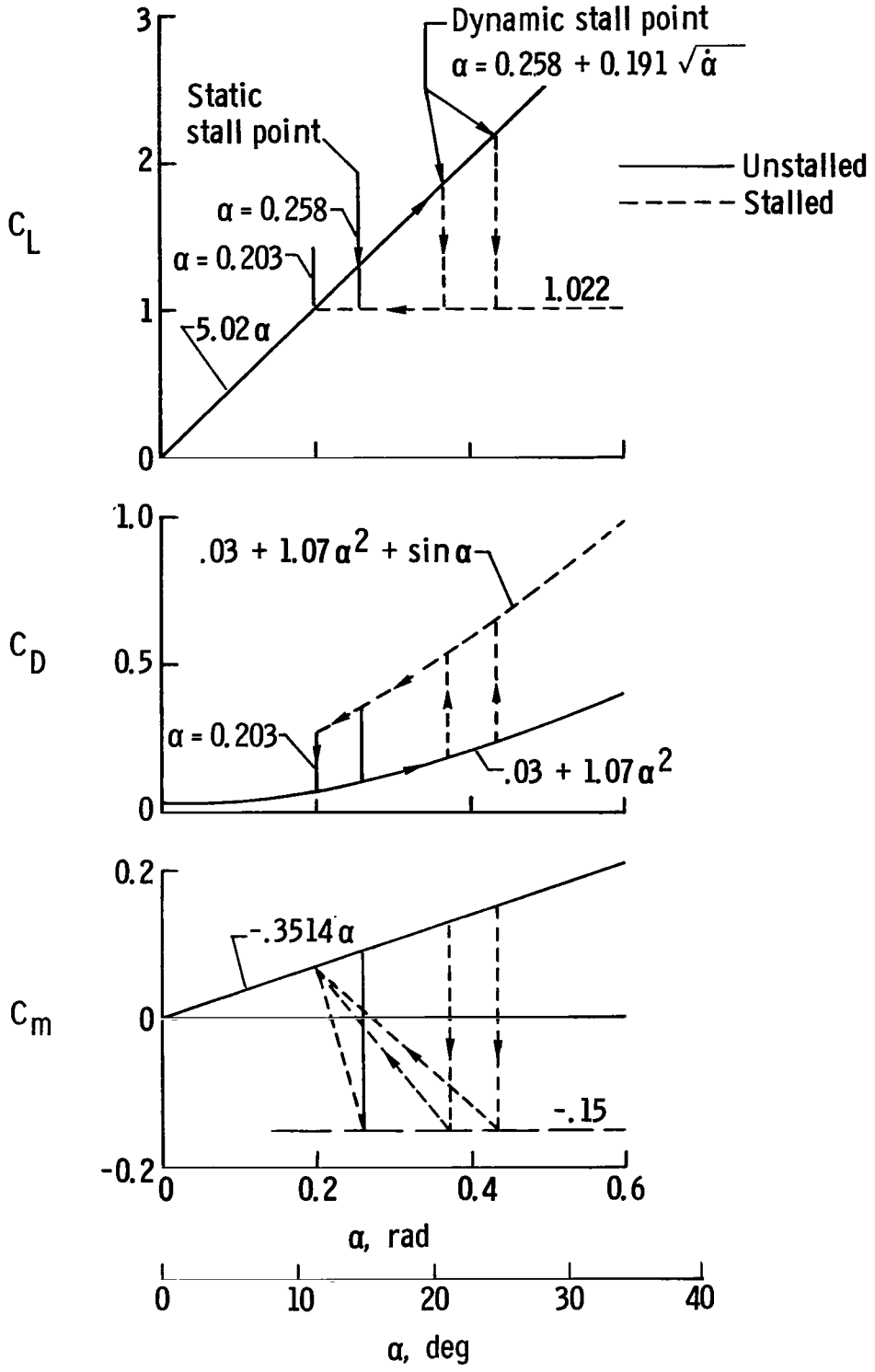

(a) Assumed aerodynamic characteristics with hysteresis, condition 1.

Figure 11.- Stall with hysteresis, condition 1.

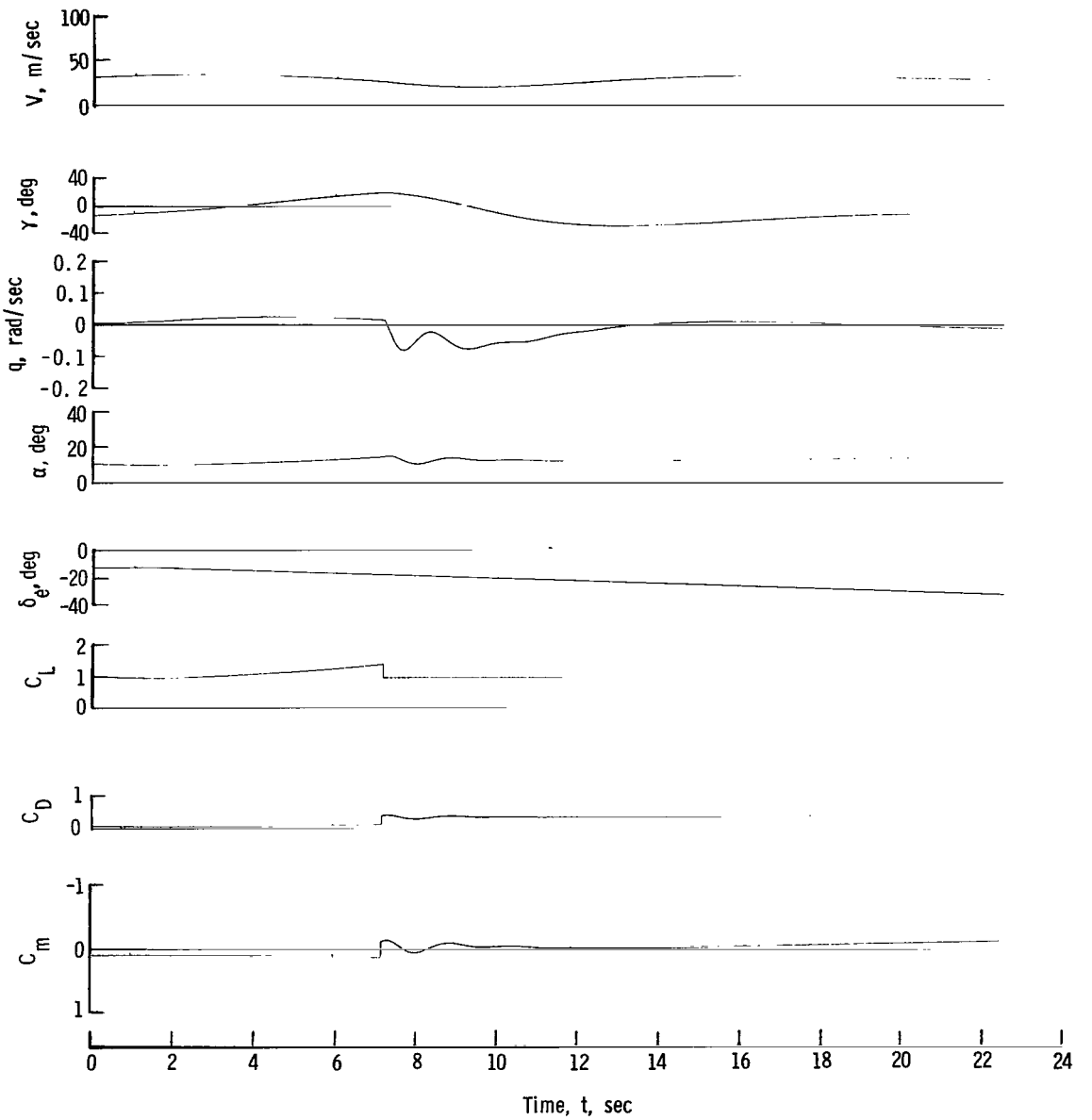

(b) Time history of stall with slow ramp input of elevator, aerodynamic characteristics with hysteresis, condition 1.

Figure 11.- Concluded.

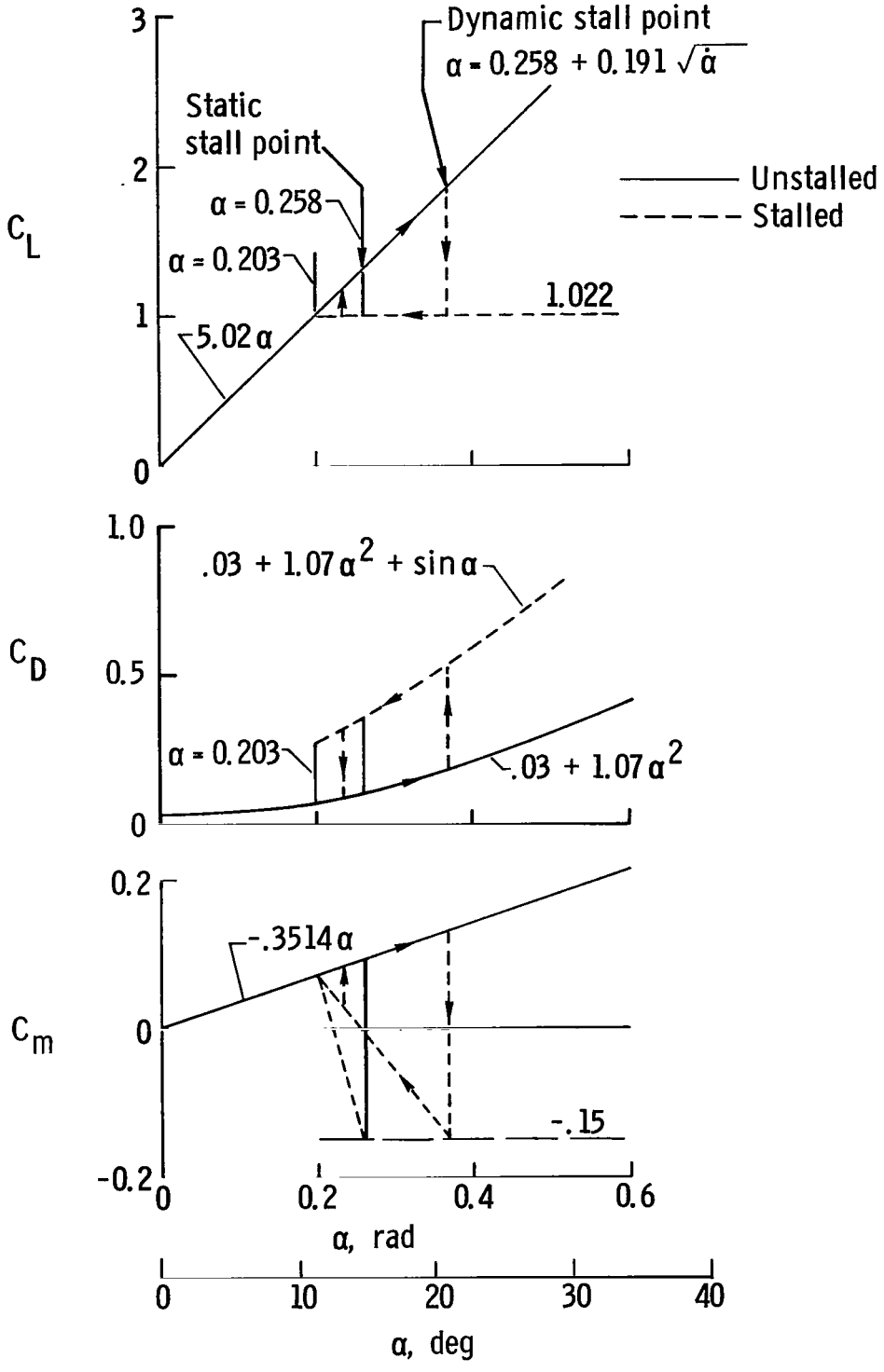

(a) Assumed aerodynamic characteristics with hysteresis, condition 2.

Figure 12.- Stall with hysteresis, condition 2.

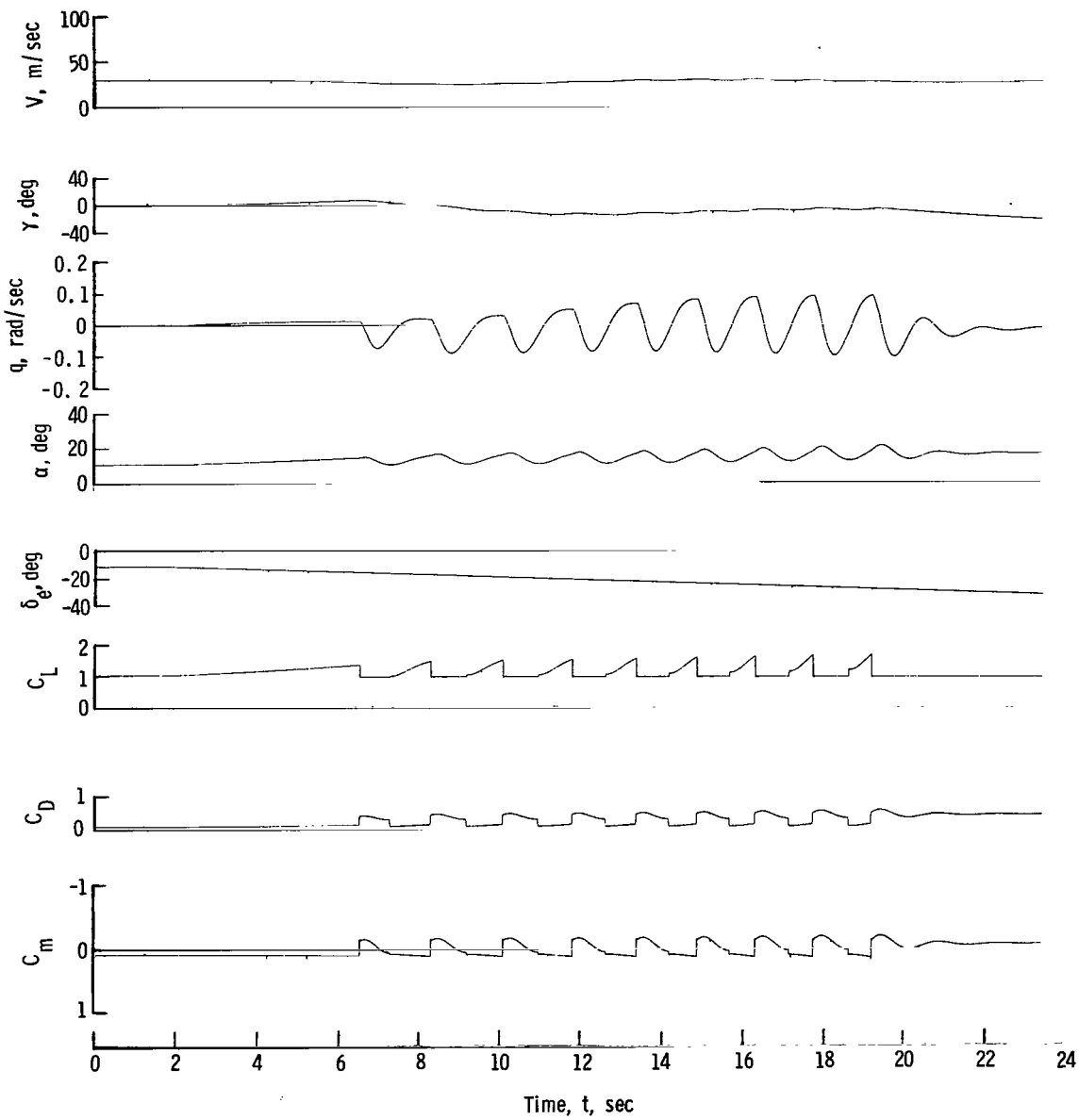

(b) Time history of stall with slow ramp input of elevator, aerodynamic characteristics with hysteresis, condition 2.

Figure 12.- Concluded.

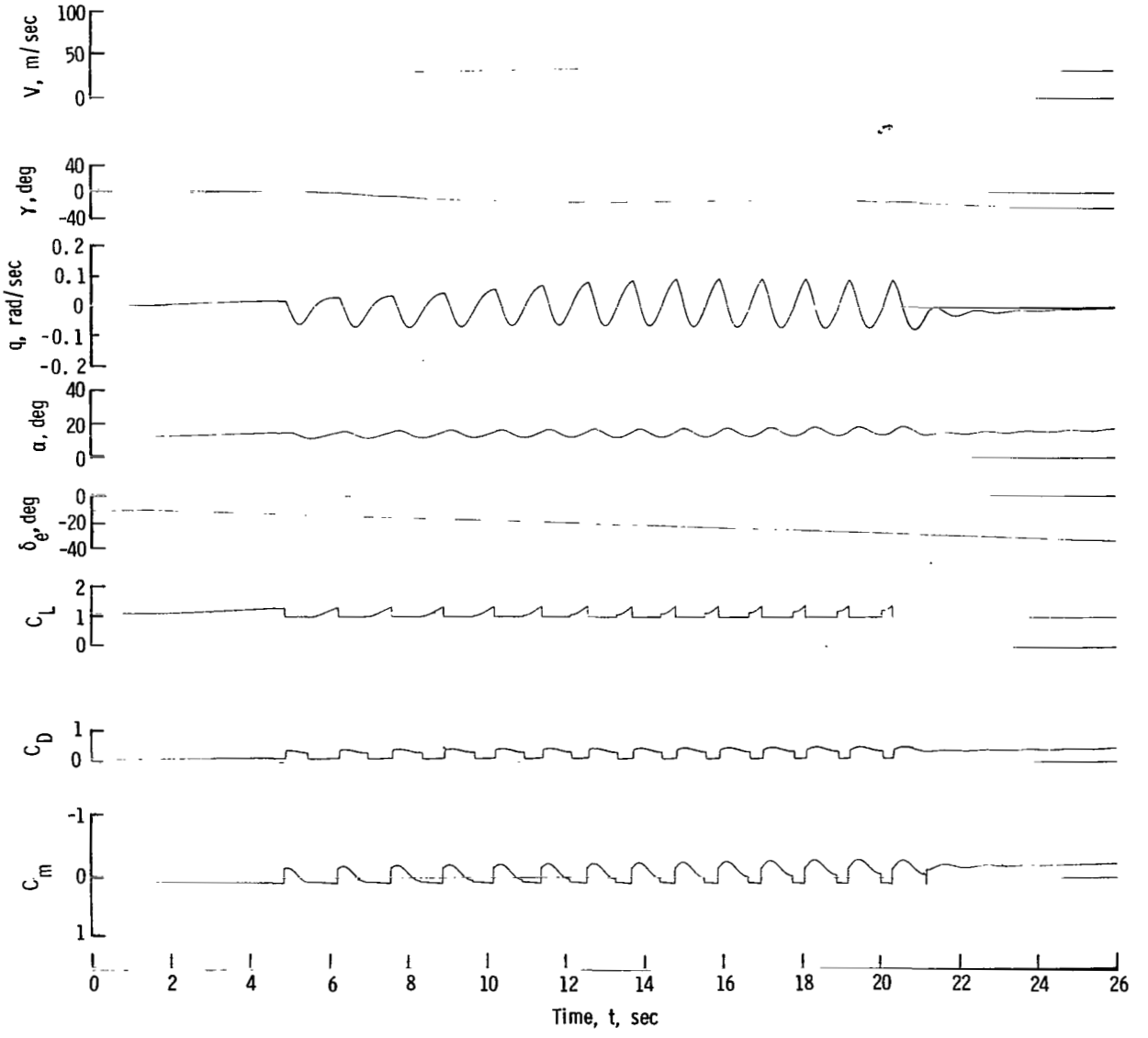

Figure 13.- Time history of stall with slow ramp input of elevator, aerodynamic characteristics with hysteresis, condition 3. Assumed aerodynamic characteristics similar to figure 12(a), except stall point is given by formula $a = 0.258 + 0.0915\dot{\alpha}$.

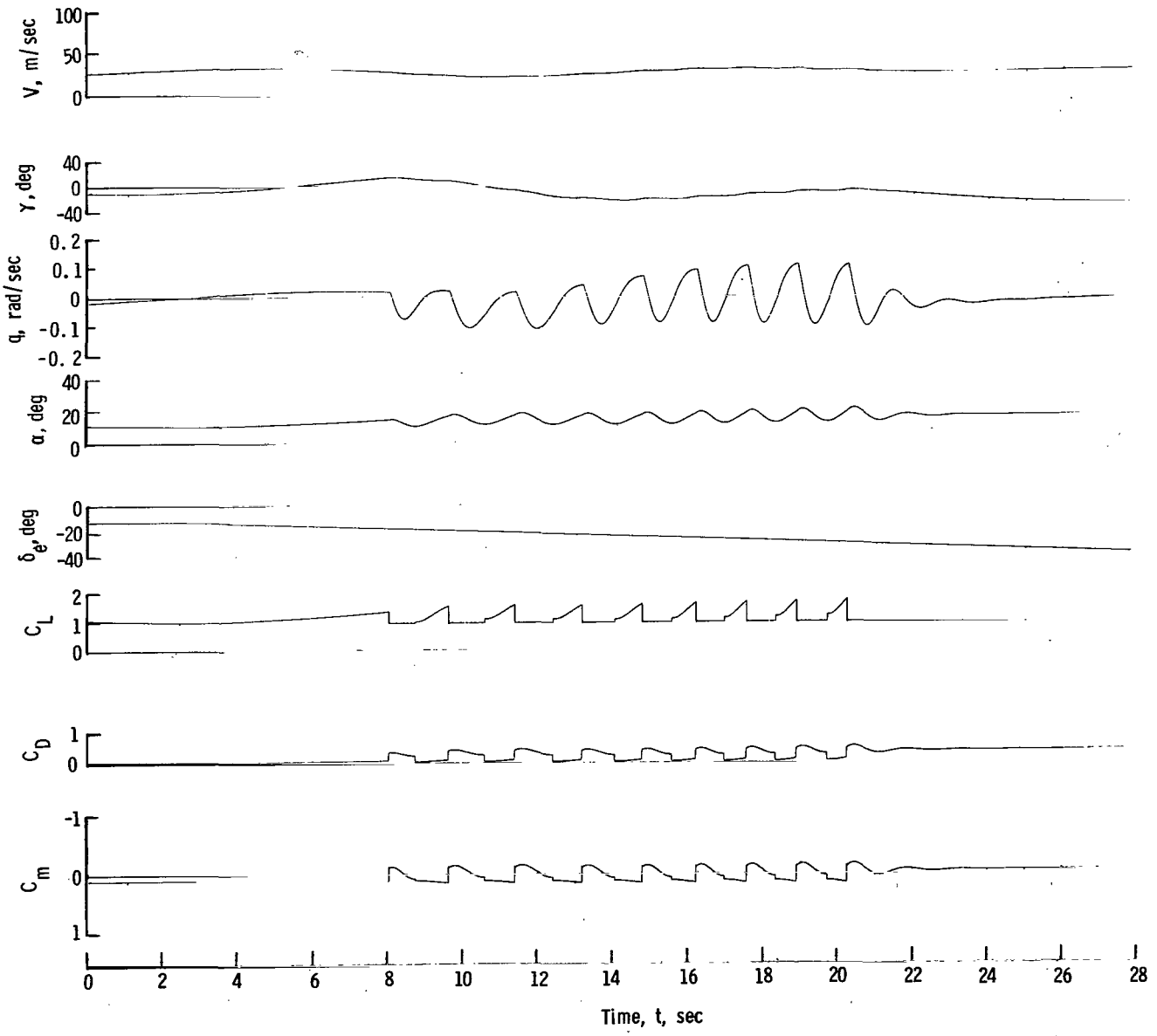

Figure 14.- Time history of stall with slow ramp input of elevator, characteristics similar to those of figure 12, except lag of downwash omitted.

1. Report No.	2. Government Accession No.	3. Recipient's Catalog No.
NASA TP-1242		

4. Title and Subtitle
SIMULATION STUDY OF THE OSCILLATORY LONGITUDINAL MOTION OF AN AIRPLANE AT THE STALL

5. Report Date
August 1978

6. Performing Organization Code

7. Author(s)
William H. Phillips

8. Performing Organization Report No.
L-12064

9. Performing Organization Name and Address
NASA Langley Research Center
Hampton, VA 23665

10. Work Unit No.
505-10-13-00

11. Contract or Grant No.

12. Sponsoring Agency Name and Address
National Aeronautics and Space Administration
Washington, DC 20546

13. Type of Report and Period Covered
Technical Paper

14. Sponsoring Agency Code

15. Supplementary Notes

16. Abstract

Hybrid simulation studies of the longitudinal motion of a straight-wing airplane at the stall have been made to investigate the effect of hysteresis in the development of lift and pitching moments on the wing as a function of angle of attack on the occurrence of longitudinal oscillations at the stall. Flight data for the simulated airplane and for various other airplanes are shown for comparison. The results show that oscillations similar to those measured in flight may be obtained by incorporating hysteresis in the lift and pitching-moment curves. More complete wind-tunnel data on the dynamic stall characteristics of an airplane would be required to predict these longitudinal oscillations more accurately.

17. Key Words (Suggested by Author(s))
Stall, longitudinal oscillations
Stall, simulation
Aerodynamics, hysteresis effects
Lift, hysteresis

18. Distribution Statement
Unclassified – Unlimited

Subject Category 08

19. Security Classif. (of this report)	20. Security Classif. (of this page)	21. No. of Pages	22. Price*
Unclassified	Unclassified	40	$4.50

*For sale by the National Technical Information Service, Springfield, Virginia 22161

NASA-Langley, 1978